

Powerful Water Masers in Active Galactic Nuclei

Philip R. Maloney

CASA, University of Colorado, Boulder, CO, 80309-0389
maloney@casa.colorado.edu

Abstract

Luminous water maser emission in the $6_{16} - 5_{23}$ line at 22 GHz has been detected from two dozen galaxies. In all cases the emission is confined to the nucleus and has been found only in AGN, in particular, in Type 2 Seyferts and LINERs. I argue that most of the observed megamaser sources are powered by X-ray irradiation of dense gas by the central engine. After briefly reviewing the physics of these X-Ray Dissociation Regions, I discuss in detail the observations of the maser disk in NGC 4258, its implications, and compare alternative models for the maser emission. I then discuss the observations of the other sources that have been imaged with VLBI to date, and how they do or do not fit into the framework of a thin, rotating disk, as in NGC 4258. Finally, I briefly discuss future prospects, especially the possibility of detecting other water maser transitions.

Keywords: galaxies: Seyfert – masers – molecular lines – radio lines: galaxies – accretion, accretion disks

1 Extragalactic Water Masers

Here I briefly review the discovery of powerful water maser sources in other galaxies; more detailed reviews, by active participants in the observation and interpretation of H₂O megamasers using VLBI, are provided in Moran et al. (1995) and Greenhill (2001).

1.1 Water Maser Emission in Galactic Sources

Maser emission in rotational lines of water – usually the $6_{16} \rightarrow 5_{23}$ transition at 22 GHz (1.35 cm) has been observed from Galactic sources for more than three decades (Cheung et al. 1969), from star-forming regions and late-type stars. The population inversion necessary to produce maser emission in this transition can be produced simply by collisions (e.g., shocks), due to the interactions between the rotational “ladders” of the H₂O molecule (de Jong 1973; see Elitzur 1992 for a detailed recent discussion). The observed luminosities are typically $L_{\text{H}_2\text{O}} \sim 10^{-3} L_{\odot}$, although the most luminous

Galactic source, W49, occasionally reaches $L_{\text{H}_2\text{O}} \sim 1 L_\odot$ (Genzel & Downes 1979)¹. Since the levels involved in the 22 GHz transition lie at energies $E/k \approx 600$ K above the ground state, the gas temperature must be at least a few hundred K in order to excite the emission.

1.2 Extragalactic Sources

The first water masers to be detected in other galaxies (e.g., M33: Churchwell et al. 1977) resembled W49, with $L_{\text{H}_2\text{O}} \sim 1 L_\odot$, and were typically found in galactic disks, in regions of star formation. These could be easily understood as extragalactic analogues of the Galactic water maser sources. However, a new and unexpected type of extragalactic H_2O maser was discovered by dos Santos & Lepine (1979) in the edge-on spiral NGC 4945. With an isotropic luminosity $L_{\text{H}_2\text{O}} \sim 100 L_\odot$, this source – which evidently arose in the galactic nucleus – was five orders of magnitude more luminous than typical Galactic H_2O masers, and was classed as a water “megamaser” ($L \sim 10^6 \times L_{\text{H}_2\text{O}}(\text{Galactic})$). Four more megamasers were found over the next 5 years, including Circinus (Gardner & Whiteoak 1982), NGC 3079 (Henkel et al. 1984a,b) and NGC 1068 and NGC 4258 (Claussen, Heiligman, & Lo 1984). Typically the emission consisted of one to a few components with velocity widths $\delta V \sim \text{few km s}^{-1}$, spread over a total velocity range $\Delta V \sim 100 \text{ km s}^{-1}$ about the systemic velocity of the galaxy V_{sys} ; an example (NGC 4945) is shown in Figure 1. Additional surveys over the next several years, mostly in late-type and infrared-luminous galaxies, failed to detect any new sources (e.g., Claussen & Lo 1986; Whiteoak & Gardner 1986).

However, all 5 of the known megamasers shared common features, as first noted by Claussen et al. (1984):

- They all were found in host galaxies with evidence of nuclear activity: three were classified as Seyferts or LINERs, and three showed unusual, extended radio emission or strong nuclear radio continuum emission;
- The maser emission was centered on the nucleus;
- In the cases of NGC 1068 and NGC 4258, the spatial diameter of the emitting regions were constrained by interferometric observations to be $d < 3.5$ and 1.3 pc, respectively (Claussen & Lo 1986).

Taking a cue from these features of the galaxies containing H_2O megamasers, Braatz, Wilson, & Henkel (1996, 1997), undertook a systematic survey of AGN for H_2O megamasers. They observed 354 active galaxies (both Seyferts and LINERs).

¹Maser luminosities are traditionally given as the isotropic value $4\pi D^2 F$, where D is the source distance and F is the line flux. Since maser emission is highly anisotropic, this can overestimate the true luminosity of an observed maser feature. However, precisely because of the anisotropy, there are almost certainly many maser features that are *not* beamed in our direction, and so the isotropic luminosity based on the observed features may provide a reasonable estimate of the actual maser luminosity.

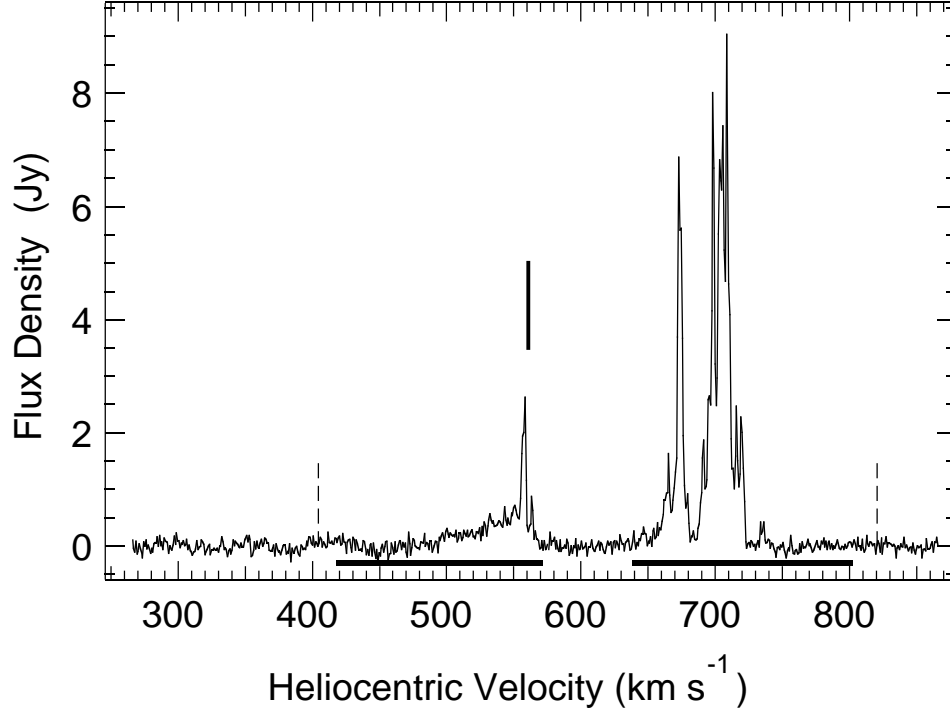


Figure 1: The spectrum of H₂O maser emission from NGC 4945, showing the spread of emission with respect to the systemic velocity (indicated by the vertical bar). From Greenhill et al. 1997a.

Ten new megamasers were found, raising the total to 16. An examination of the statistics in both distance-limited ($cz < 7000 \text{ km s}^{-1}$) and sensitivity-limited ($L_{\text{H}_2\text{O}} > 2 L_{\odot}$) samples leads to a remarkable result:

In the distance-limited sample:

- 7% (10/141) Sy 2 detected
- 7.5% (5/67) LINERs detected
- 0% (0/57) Sy 1 detected

For the sensitivity-limited sample, these percentages become:

- 14% (10/73) Sy 2 detected
- 10% (5/52) LINERs detected
- 0% (0/30) Sy 1 detected

The fraction of H₂O megamasers in AGN is *not* small, provided that Type 1 Seyferts are excluded. Hence either: (1) Sy 1 don't possess nuclear molecular gas in which the physical conditions are suitable for masing, or (2) the megamasers in Sy 1 galaxies are systematically beamed *away* from us.

Since the Braatz et al. survey, eight more megamasers have been discovered², bringing the current total to 24 (see the list in Moran, Greenhill, & Herrnstein 1999, plus Mrk 348 [Falcke et al. 2000b] and NGC 6240 [Hagiwara, Diamond, & Miyoshi 2002; Nakai, Sato, & Yamauchi 2002]). All of the sources are in galaxies classified as either Sy 2 (14/24) or LINERs (10/24). In all cases the emission is confined to the nucleus (although in the case of the merger NGC 6240, the location of the nucleus is somewhat problematic). The survey reported by Greenhill et al. (2002) detected only one new source out of 131 galaxies searched; however, only about 50 of these sources are classed as Sy 2 or LINERs. Nine megamaser sources have now been imaged using VLBI; the results will be discussed in §4 and 5.

2 The origin of water megamasers

As mentioned above, the $6_{16} \rightarrow 5_{23}$ transition of H_2O at 22 GHz can be driven to mase by collisions, provided that the densities and temperatures are high enough ($n_{\text{H}_2} \gtrsim 10^7 \text{ cm}^{-3}$, $T \gtrsim 400 \text{ K}$, respectively) to excite the levels involved, and that the levels deviate from thermodynamic equilibrium, which implies that $n_{\text{H}_2} \lesssim 10^{11} \text{ cm}^{-3}$, and that the gas kinetic temperature is substantially higher than the temperature of the radiation field in the mid- to far-infrared, where the pure rotational transitions connecting the levels occur. In the Galactic sources of water maser emission, namely, star-forming regions and the atmospheres of late-type stars, there is little doubt that the necessary conditions are produced by shock waves. However, the unique association between water megamasers and active galactic nuclei suggests that there is another mechanism at work in many if not all of these sources. As I will show below, the best explanation for the majority of the sources is likely to be maser emission arising in dense gas that is being irradiated by X-rays from the AGN. Before discussing the maser emission, I will first digress briefly to discuss the characteristics of these *X-Ray Dissociation Regions*.

2.1 X-Ray Dissociation Regions

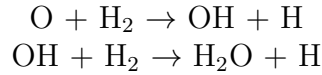
Consider a power-law spectrum incident on a layer of dense gas: after spectral filtering through absorption in the gas, only X-rays, with energies E above a few hundred eV, are left. This is very significant for active galactic nuclei, because for typical AGN spectra, approximately equal amounts of energy per decade are available. Hence the hard X-ray ($E \gtrsim 1 \text{ keV}$) luminosity L_x is roughly one-tenth of the bolometric luminosity L_{bol} . These hard X-rays can have a profound influence on the physical state of the ISM in a galaxy with an active nucleus, since photons with $E \gtrsim 1 \text{ keV}$ have small cross-sections for absorption, and hence large mean free paths, but large E/photon , so that the local energy input rates when the photons are absorbed are substantial. Much of the locally deposited energy goes into heating the gas; the remainder goes into ionization and

²A database of galaxies that have been searched for 22 GHz water maser emission is maintained by Jim Braatz, and is available at <http://www.gb.nrao.edu/~jbraatz/H2O-list.html>.

excitation (Maloney, Hollenbach, & Tielens 1996). For a typical ($f_\nu \propto \nu^{-\alpha}$, with $\alpha \sim 1$) AGN X-ray spectrum, the ionization and heating rates fall with the column density N only as $\sim N^{-1}$. This is in marked contrast to the *photodissociation regions* (PDRs) produced by FUV photons (Tielens & Hollenbach 1985), in which the heating rates decline exponentially with column density since the absorption is produced by dust. This means that the column density in an XDR can be large, and therefore that the volume around a luminous AGN occupied by the XDR (i.e., where X-rays dominate the ionization and heating rates) can be substantial. For typical AGN spectra, the ionization and heating rates are always dominated by the lowest energy photons that have yet to be significantly attenuated. The physical state of the gas is described to lowest order by an effective X-ray ionization parameter ξ_{eff} , related to the usual ratio of X-ray flux to gas density, but including a scaling with column density that accounts for the optical thickness of the gas to the incident radiation. This scaling depends weakly on the spectral index but is generally close to N^{-1} , as noted above (see Maloney, Hollenbach, & Tielens 1996 for details).

2.2 Water Maser Emission from Dense X-Ray Irradiated Gas in AGN

High-pressure XDRs prove to be ideal locations for the production of luminous water maser emission (Neufeld, Maloney, & Conger 1994, hereafter NMC). Provided the gas temperature is above ~ 400 K but is not so high ($T \sim 4000$ K) that H_2 is destroyed, the reaction network



forms water very efficiently. This is also the approximate temperature criterion for collisionally exciting the 22 GHz transition, as discussed earlier. An X-ray-irradiated layer of dense gas generally undergoes a phase transition from warm, atomic gas to cooler, molecular gas. An example is shown in Figure 2. The temperature plummets from $T \sim 6000$ K to $T \sim 1000$ K at the transition, while the H_2 abundance climbs from \sim a few $\times 10^{-5}$ to \sim ten percent. The water abundance relative to hydrogen jumps from negligible values ($x_{\text{H}_2\text{O}} \lesssim 10^{-12}$) to \sim a few $\times 10^{-6}$, and then climbs to $\sim 10^{-4}$ before starting to decline as the temperature drops with increasing column density. (The initial rise in temperature following the transition is due to the effects of radiative trapping, which acts to reduce the effective cooling rate per unit volume as the optical depths in important cooling transitions increase; this effect is eventually outweighed by the continued decline in the gas heating rate with increasing N .)

The physical conditions just past the phase transition are ideal for producing water maser emission over a very broad range of pressures, $P/k \approx 10^{10} - 10^{13}$ cm $^{-3}$ K. Figure 3 (from NMC) shows a more detailed look at the temperature and water abundance as a function of depth (rather than column density) into an X-ray-irradiated slab. Also shown is the maser volume emissivity in saturation, Φ_{sat} . The maser volume emissivity

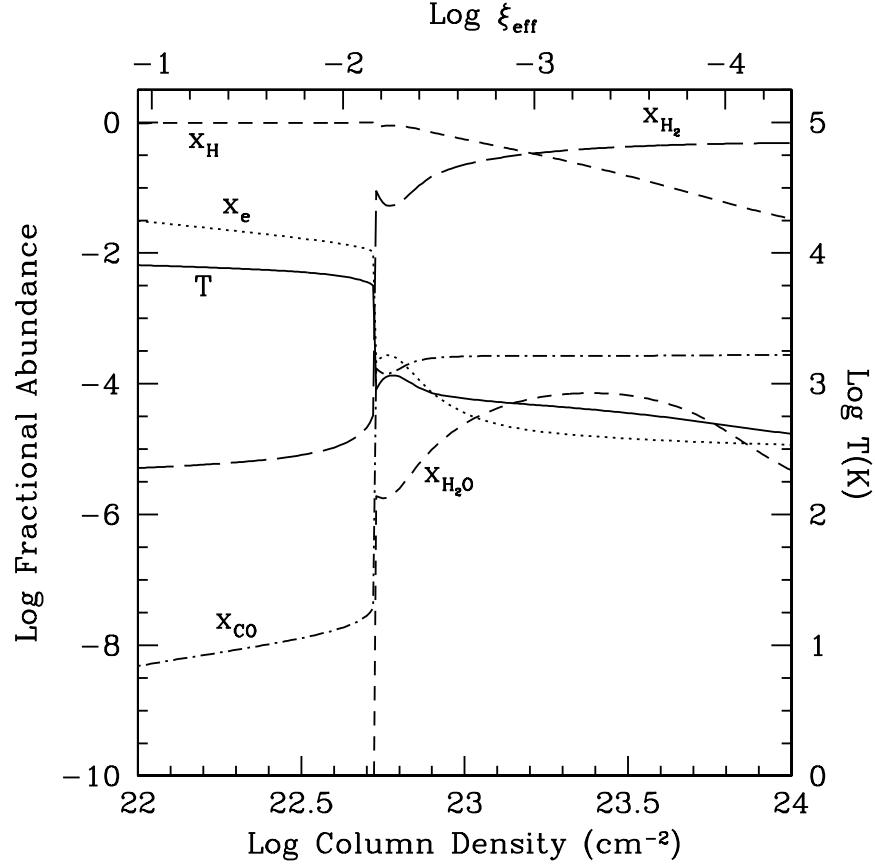


Figure 2: Thermal and chemical structure of an isobaric XDR. This model assumes an X-ray source with a hard X-ray (1–100 keV) luminosity of 10^{43} erg s $^{-1}$ and an X-ray spectral index $\alpha = 0.7$ at a distance of 1 pc. The pressure has been fixed at $P/k = 10^{11}$ cm $^{-3}$ K. The gas temperature, electron fraction, and the abundances of several important species (relative to the total hydrogen density) are plotted as a function of column density into the XDR (bottom axis) and X-ray ionization parameter ξ_{eff} (top axis).

is simply the rate at which maser photons (in a particular transition) are generated per unit volume; this rate can never be larger than the rate when the maser is fully saturated (i.e., when the maser radiation itself controls the population inversion responsible for maser action; see for example Neufeld & Melnick 1991; Elitzur 1992). To the right of the vertical dotted line in this panel, the maser action is quenched by radiative trapping in the non-masing rotational transitions. However, this calculation ignored the role of dust in the radiative transfer. As pointed out by Collison & Watson (1995; see also Neufeld 2000), the presence of dust can be very important for these X-ray-powered masers, because dust absorption sets a lower limit to the escape probability for the far-infrared rotational transitions, and thus acts to inhibit quenching of the maser emission, provided that the dust is substantially cooler than the gas; otherwise the radiation from the dust would be important. This is unique to these XDR masers, because only there can the column densities become large enough that the far-infrared dust optical depths become significant. The importance of dust depends on the pressure in the XDR, and is negligible for $P/k \gtrsim 10^{12} \text{ cm}^{-3} \text{ K}$. This is because with increasing pressure the location of the transition to the molecular regime moves to smaller column density; since the column density at the transition sets the column density scale on which the ionization and heating rates decline, with increasing P the XDR becomes more compressed in column density, so the importance of dust in the radiative transfer diminishes.

As shown by NMC, the resulting water maser luminosities from XDRs can be substantial, reaching $L_{\text{H}_2\text{O}} \sim 10\text{s to } 100\text{s } L_{\odot}$ per pc^2 of irradiated area. Since this is the luminosity range seen in the megamaser galaxies, with the exception of the so-called “gigamaser” source (Koekemoer et al. 1995), which is an order of magnitude more luminous, it is evident that XDRs *can* explain the association of H_2O megamasers with AGN, provided that areas of only $\sim 1 \text{ pc}^2$ are being irradiated by hard X-rays from the AGN. Since the obscuring “tori” inferred to be present in Type 2 Seyferts (see Antonucci 1993 for a review) were also inferred to be $\sim \text{pc}$ -scale objects, they naturally provided the requisite surface areas to explain the megamaser luminosities, without appeal to any special geometries.

3 Imaging 1: NGC 4258

Further progress in understanding H_2O megamasers would depend on imaging the maser emission. With the advent of the Very Long Baseline Array (VLBA), it became possible to obtain very high resolution interferometric images of the 22 GHz emission in sufficiently bright megamaser sources. The first such galaxy to be observed was the nearby ($D \approx 7 \text{ Mpc}$), LINER spiral NGC 4258, which has a 22 GHz line luminosity $L_{\text{H}_2\text{O}} \approx 85 L_{\odot}$. Most strikingly, NGC 4258 was already known from single-dish observations (Nakai et al. 1993) to show an enormous velocity spread in its maser emission, with ΔV up to $\pm 1000 \text{ km s}^{-1}$ with respect to the systemic velocity. Combined with the already established concentration of the emission to the nucleus from earlier VLA observations (Claussen & Lo 1986), this strongly suggested that material very deep in a potential well – such as gas in proximity to a massive black hole – could be involved

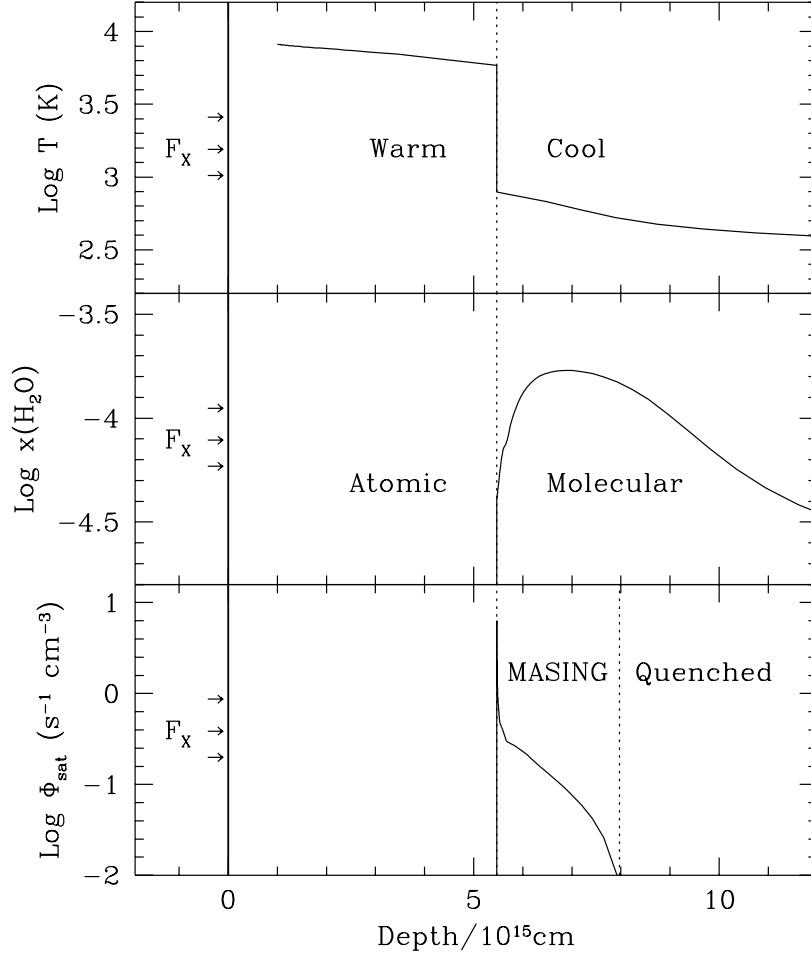


Figure 3: As Figure 2, except plotted as a function of depth rather than column density. F_x denotes the incident hard X-ray flux. In addition to temperature and water abundance, the bottom panel shows the maser emissivity Φ_{sat} (photons $\text{cm}^{-3} \text{sec}^{-1}$); see the text for definition. From NMC.

in the emission.

NGC 4258 was first observed using VLBI by Greenhill et al. (1995). Only the systemic emission was imaged; nevertheless, these observations already revealed some of the key features discussed below. Maser emission over the full velocity range was imaged using the VLBA by Miyoshi et al. (1995). The results, summarized in Figure 4 (from Bragg et al. 2000), are quite remarkable. Among the notable features:

- The maser emission does not arise from the inner face of an X-ray-irradiated torus; instead, it is produced in a thin, warped disk or annulus, with inner and outer edges at 0.14 and 0.28 pc. This distance scale corresponds to an inner edge at 38,000 Schwarzschild radii for the mass of the central black hole (see below). The disk is extremely thin: the maser emission is unresolved in the vertical direction, implying that the thickness of the masing layer is less than 10^{15} cm (Moran et al. 1995).
- The rotation curve is Keplerian to better than 1%. This places stringent limits on the nature of the central mass concentration (Maoz 1995): the central mass $M = 3.9 \times 10^7 M_\odot$ within 0.14 pc. This implies that the central mass density $\rho > 3.4 \times 10^9 M_\odot$. Combined with the limits on deviation from Keplerian motion, this rules out a stellar cluster as the central object. If the cluster were composed of stars or stellar remnants with masses above $M \sim 0.03 M_\odot$, the evaporation timescale $t_{\text{evap}} \ll t_H$, the Hubble time. For a cluster made up of brown dwarfs or other low mass objects with $M < 0.03 M_\odot$, the collisional timescale $t_{\text{coll}} \ll t_H$. In addition, a stellar density cusp around a low-mass black hole is also ruled out. Hence NGC 4258 provides compelling evidence for the existence of a supermassive black hole in a galactic nucleus.
- Since we know the mass of the central object and the associated X-ray luminosity (Makishima et al. 1994) quite accurately, we can make the first reliable determination of the fractional Eddington luminosity in an AGN, subject only to uncertainty in the hard X-ray to bolometric luminosity ratio. This turns out to be quite small, with $L/L_{\text{Edd}} \sim 10^{-4}$.
- Observations of centripetal acceleration ($a \approx 9 \text{ km s}^{-1} \text{ yr}^{-1}$: Haschick, Baan, & Peng 1994; Greenhill et al. 1995a; Nakai et al. 1995) or proper motion ($\mu \approx 32 \mu\text{as yr}^{-1}$: Herrnstein 1997; Herrnstein et al. 1999) of systemic velocity features allow a purely *geometric* determination of the distance to NGC 4258 ($D = 7.3 \pm 0.3 \text{ Mpc}$); both methods give the same answer. The tight limit on the distance quoted here comes from the data set analyzed in the last two of these references, which contains multiple epochs of observation from 1994 to 1997. The uncertainties are contributed nearly equally by the statistical errors (i.e., the precision with which a and μ can be determined, which is limited mainly by the difficulty in identifying and tracking individual features) and the uncertainties in the disk model (chiefly the projected disk angular velocity at the radius of the systemic features).
- Observations of centripetal acceleration of the systemic and high-velocity features (the latter having $a \lesssim 1 \text{ km s}^{-1} \text{ yr}^{-1}$: Bragg et al. 2000) confirm that the

geometry inferred for the masers (shown in Figure 4) is correct; the scatter of the high-velocity features about the disk midline, as constrained by the upper limits on a , is only a few degrees, while the systemic velocity features lie within a very narrow range of radii (approximately 0.01 pc spread about a mean radius $R = 0.14$ pc). This latter conclusion is supported by the essentially linear variation of velocity with impact parameter b for the systemic velocity features (with a gradient $dv/db \simeq 0.26 \text{ km s}^{-1} \mu\text{as}^{-1}$); this behavior is expected as the projection of orbital velocity onto our line of sight changes with impact parameter (Miyoshi et al. 1995). Calculation of the implied radius for the enclosed mass places the systemic velocity features at the same mean radius as inferred from the centripetal accelerations.

- Compact continuum emission has been detected at 22 GHz (Herrnstein et al. 1997). The peak of the emission is located about 0.015 pc north of the dynamical center of the disk. Herrnstein et al. suggest that this is the base of the northern jet of the symmetric pair seen on parsec to kiloparsec scales in the radio and X-ray, and detect a much weaker southern component, at somewhat greater distance from the disk center, which they argue is attenuated by free-free absorption in the warm atomic layer on that side of the disk. Assuming the VLBI jet is intrinsically symmetrical, the failure to detect the southern component at the same offset (0.5 mas) as the peak in the northern jet suggests that the free-free optical depth is $\gtrsim 2$. Herrnstein et al. argue that the systemic velocity masers are amplifying the southern jet emission, an argument that is supported by the correlation of the maser flux density with the continuum flux density of the northern jet emission; this in turn implies that the jet is symmetric, as assumed.
- By searching for Zeeman-splitting-induced circular polarization of the 22 GHz water maser emission, Herrnstein et al. (1998) derived an upper limit of 300 mG to the magnetic field strength in the disk at a radial distance of 0.2 pc. This upper limit is about four times larger than the value required for an equilibrium disk supported by magnetic pressure. However, it is still significant because one cannot rule out *a priori* the possibility that the masers trace a thin layer in a much thicker accretion disk. This upper limit to B can also be used to place an upper limit to the mass accretion rate through the disk, under the assumption of equipartition; unfortunately, this method at present is not restrictive enough to discriminate between competing models for the disk (see §3.2).
- The angle over which the maser emission from NGC 4258, which is beamed in the plane of the disk, is detectable can be determined from the velocity extent of the emission near the systemic velocity, compared to the rotation velocity. This gives a beaming angle of 8° (Miyoshi et al. 1995). One can also estimate the observable solid angle from the magnitude of the disk warp, which has an angular thickness much greater than the thickness of the maser layer, and gives a “warp angle” of approximately 11° . Using either number, the observed solid angle is consistent with all Seyferts and LINERS containing such maser disks,

but only those in which our line of sight intercepts the (nearly edge-on) disk are detectable. This suggests that the masing regions are either identical with, or physically associated with, the obscuring material (the TORUS³) around the AGN.

3.1 Deriving the Mass Accretion Rate

The maser emission from NGC 4258 arises in what is quite clearly the accretion disk around the central black hole. It is perhaps remarkable that the first direct detection of an accretion disk around a supermassive black hole was obtained in a molecular transition, using ground-based telescopes. We can also use the H₂O maser emission to infer the mass accretion rate through the disk (Neufeld & Maloney 1995; NM95). First, however, we must return briefly to the results of NMC.

Figure 5 shows a phase diagram for dense, X-ray-irradiated gas. The abundance of water and the gas temperature are plotted as a function of an X-ray ionization parameter, here written as $F_5/(N_{24}^{0.9}\tilde{P}_{11})$, where the incident *unattenuated* X-ray flux $F_x = 10^5 F_5 \text{ erg cm}^{-2} \text{ s}^{-1}$, $N_{\text{att}} = 10^{24} N_{24} \text{ cm}^{-2}$ is the attenuating column density to the source of X-rays, and the gas pressure $P = 10^{11} k \tilde{P}_{11} \text{ dyne cm}^{-2}$. (This diagram was actually calculated by varying F_x , but the results will scale approximately with N_{att} and P as indicated.) Note that there are actually two main branches, corresponding to the warm, atomic phase and the cooler, molecular phase. Over a range of ionization parameter, both equilibria are present, allowing for the possibility of a two-phase medium with the warm atomic and cooler molecular phases coexisting. The important point is that the upper branch in the temperature plot (the warm atomic phase) does not exist for ionization parameters smaller than a critical value of about 6.5. This means that for a fixed flux and shielding column, there is a maximum pressure for which the warm atomic phase can exist; at pressures higher than this, the gas *must* be in the molecular phase.

To apply this to NGC 4258, we need a model of the accretion disk. Since the masers appear to arise in a thin disk, model it as one: a Shakura-Sunyaev α -disk (Shakura & Sunyaev 1973), but with a warp (which is actually crucial, as shown below). In this model the kinematic viscosity ν is assumed to be proportional to the product of the sound speed c_s and the disk scale height H , with the constant of proportionality designated α (see Frank, King & Raine 1992 for a review of the theory of accretion disks). The actual source of viscosity has been a mystery for many years but is now generally believed to be provided by the magnetorotational instability (Balbus & Hawley 1991).

Because of the warp, portions of the disk see the central X-ray source. In the obliquely illuminated region between 0.14 and 0.28 parsecs (the masing annulus), X-ray heating dominates over viscous heating by about an order of magnitude, and the disk is nearly isothermal. We therefore model the disk using the α prescription for viscosity, but the temperature is set by the X-ray heating rather than viscous heating

³Thick Obscuration Required by Unified Schemes: see Conway 1999.

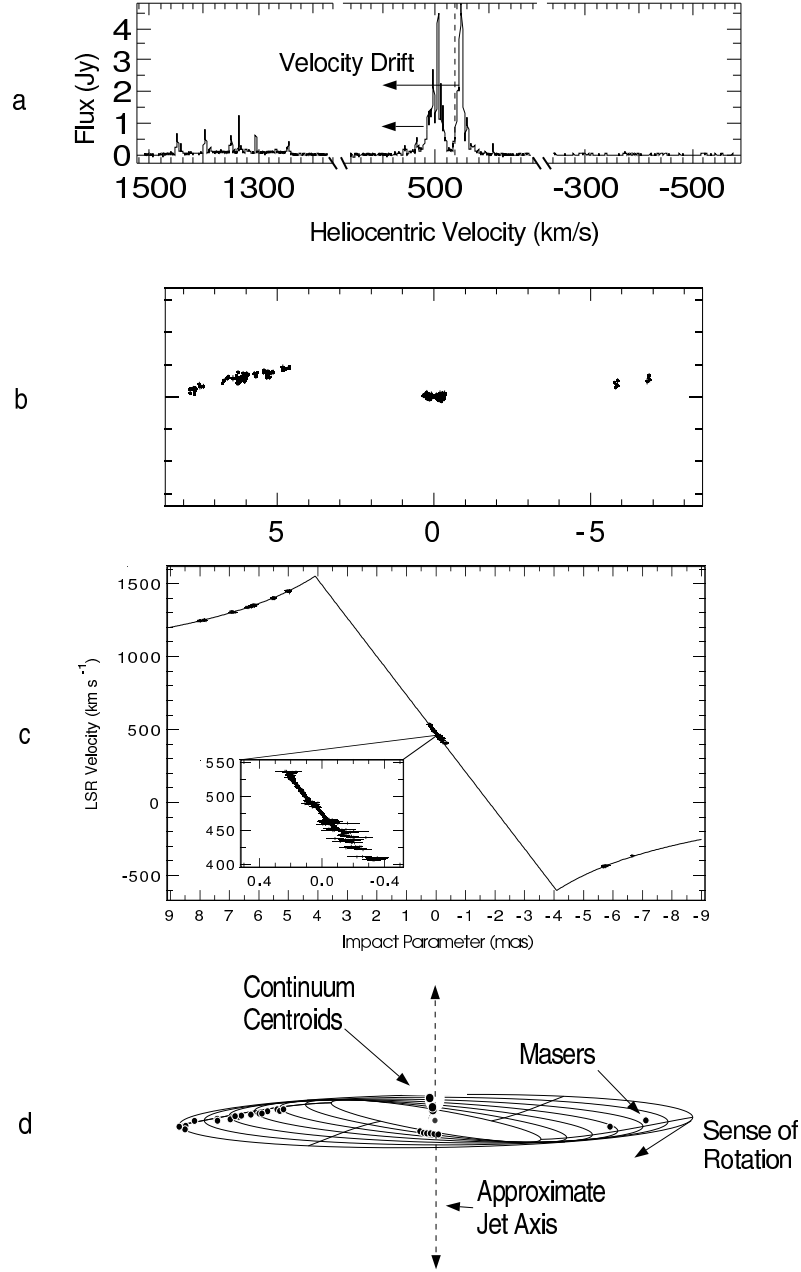


Figure 4: The maser disk in NGC 4248, as inferred from VLBA observations. The top panel shows a typical spectrum of this system, with the direction of velocity drift of the features indicated. The second panel shows the projection of the maser spots on the plane of the sky. The third shows the velocities of the spots as a function of impact parameter; the solid line is a Keplerian rotation curve. The bottom panel shows the inferred structure of the system. From Bragg et al. 2000.

as in a standard α -disk. Ignoring self-gravity, the disk scale-height is

$$H = \frac{c_s}{V_{\text{orb}}} R = 2.6 \times 10^{14} \frac{T_3^{1/2} R_{0.1}^{3/2}}{M_8^{1/2}} \text{ cm} \quad (1)$$

where the disk temperature $T = 10^3 T_3$ K, the disk radius is $R = 0.1 R_{0.1}$ pc, and the mass of the central black hole $M_{\text{bh}} = 10^8 M_8 M_\odot$. Hence the disk is expected to be extremely thin, as observed. The disk midplane pressure (P/k) is

$$\tilde{P} = 1.3 \times 10^{11} \frac{M_8 \dot{M}_{-5}}{\alpha R_{0.1}^3} \text{ cm}^{-3} \text{ K}. \quad (2)$$

where the mass accretion rate through the disk $\dot{M} = 10^{-5} \dot{M}_{-5} M_\odot \text{ yr}^{-1}$.

If we now take the critical pressure derived from the results of NMC, with the flux expressed in terms of the luminosity of the central X-ray source and the disk radius, scaled to appropriate values for NGC 4258, we have that the critical pressure for molecule formation is

$$\tilde{P}_{\text{cr}} \approx 3.3 \times 10^{10} \frac{L_{41}}{R_{0.1}^2 N_{24}^{0.9}} \text{ cm}^{-3} \text{ K}. \quad (3)$$

Equating these two expressions gives the critical radius for molecule formation:

$$R_{\text{cr}} = 0.04 \frac{(\dot{M}_{-5}/\alpha)^{0.81} M_8^{0.62}}{L_{41}^{0.43} \mu^{0.38}} \text{ pc} \quad (4)$$

where μ corrects for oblique illumination at an angle $\cos^{-1} \mu$. In writing this expression we have also assumed that the disk itself provides all of the shielding column density, although violation of this assumption could only change \dot{M} by at most a factor of two. Notice that from equation (2), the disk midplane pressure falls with radius as R^{-3} , whereas the X-ray flux from the AGN will decrease as R^{-2} . This means that the X-ray ionization parameter actually *increases* outwards, which means the transition from a molecular to an atomic disk should be identified with the *outer* edge of the masing annulus. Plugging in the values appropriate for NGC 4258 ($M_8 = 0.39$, $L_{41} = 0.4$, and $\mu \approx 0.25$, and $R = 0.28$ pc), and solving equation (4) for the mass accretion rate, we get

$$\frac{\dot{M}}{\alpha} \approx 7 \times 10^{-5} M_\odot \text{ yr}^{-1}. \quad (5)$$

With the inferred mass accretion rate, the mass of the masing disk is only $\sim 10^3 M_\odot$, and the neglect of the disk self-gravity is justified.

Why is there an *inner* edge to the masing region? In NM95, it was speculated that this is because the disk actually flattens out interior to 0.14 pc, so that it is no longer illuminated by the X-ray source. In this case the temperature will be determined by viscous heating, and this will in general be too low to produce abundant water or

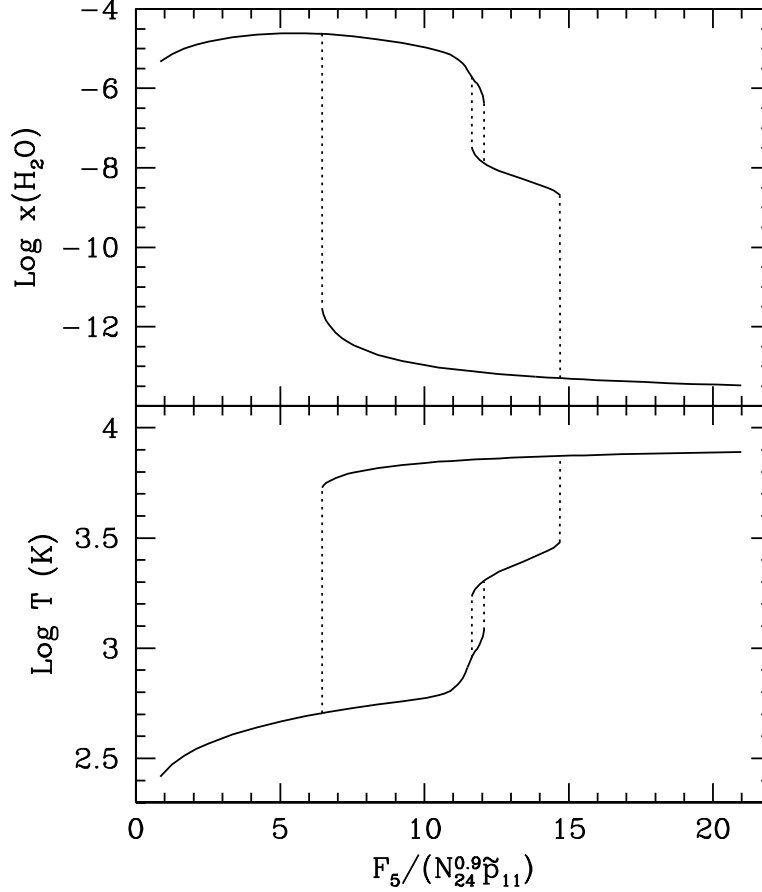


Figure 5: Phase diagram for dense X-ray irradiated gas. The water abundance relative to hydrogen and the gas temperature are plotted as a function of the X-ray ionization parameter $F_5/(N_{24}^{0.9}\tilde{P}_{11})$, where the incident X-ray flux $F_x = 10^5 F_5 \text{ erg cm}^{-2} \text{ s}^{-1}$, $N_{\text{att}} = 10^{24} N_{24} \text{ cm}^{-2}$ is the attenuating column density (i.e., the column density of gas that is neutral enough to absorb X-rays at the energies of interest) to the source of X-rays, and the gas pressure $P = 10^{11} k \tilde{P}_{11} \text{ dyne cm}^{-2}$. The upper and lower branches correspond to the warm atomic and cooler molecular phases, respectively, in the bottom panel, and are reversed in the upper panel. The existence of the intermediate temperature phase is very sensitive to radiative trapping of cooling lines, and it probably does not occur in real tori or disks around AGN. Over the range of ionization parameter in which both branches exist, a two-phase medium is possible.

maser action (see further discussion on this point below)⁴. Such a disk geometry is expected in the case of radiation-driven warping (Pringle 1996; Maloney, Begelman, & Pringle 1996) since in this case the warp grows from the outside inwards. Whatever the mechanism producing the warp, its presence is crucial in the X-ray-powered maser model, since it is the warp that allows the central source to irradiate the disk and produce the maser emission.

The physical conditions in the disk inferred in this model are shown in Figure 6. Beyond the critical radius at 0.28 pc, the disk is forced by the X-ray irradiation into the warm atomic state; the temperature is about 8000 K, and the scale height is about $H \sim 5 \times 10^{15}$ cm. Molecular abundances are negligible. At the critical radius, the pressure is just high enough at the midplane to force the gas into the molecular phase. With decreasing radius the thickness of the molecular zone increases as a larger fraction of the disk is above the critical pressure; the temperature in the molecular zone will rise with increasing z -height above the midplane. Interior to 0.14 pc, where the warp flattens out, the disk temperature drops below 100 K, and masing ceases.

If we assume that $L_x/L_{bol} \sim 0.1$, as is typical for AGN, the derived mass accretion rate implies that rest-mass energy is converted to radiation with a radiative efficiency

$$\epsilon \sim 0.1/\alpha \quad (6)$$

(assuming steady accretion over the time it takes material to reach the black hole from 0.28 pc; the validity of this assumption is rather uncertain, as discussed briefly below). This in turn indicates that the low fractional Eddington luminosity of NGC 4258 is due to the low mass accretion rate onto the central black hole, and *not* due to low radiative efficiency of the accreting material. Also, although we do not know *a priori* where our line of sight to the X-ray source intercepts the disk, the column densities inferred for the disk strongly suggest that our sightline passes through the disk just at the edge of the molecular zone (NM95).

3.2 Alternative models

The model of Neufeld & Maloney (1995), as outlined above, is essentially the “what-you-see-is-what-you-get” model: since the maser emission appears to arise in a thin, warped, disk, assume that this is in fact the case, with the warping of the disk allowing these regions of the disk to see the central X-ray source, which then powers the maser emission by a well-understood process (NMC). Unsurprisingly, in view of the uniquely detailed information on an accretion disk around a supermassive black hole provided by the maser observations, a number of additional models have been proposed. These will be briefly discussed here.

Maoz & McKee (1998) (MM98) proposed that rather than X-ray heating, the maser

⁴Although maser action in the 22 GHz line requires that the gas density be less than $n \sim 10^{10} \text{ cm}^{-3}$, it is unlikely that the inner edge is produced by the increase of the density with decreasing radius. As the midplane density rises, the masing layer will simply move to a greater height above the disk. See also the discussion in §3.2

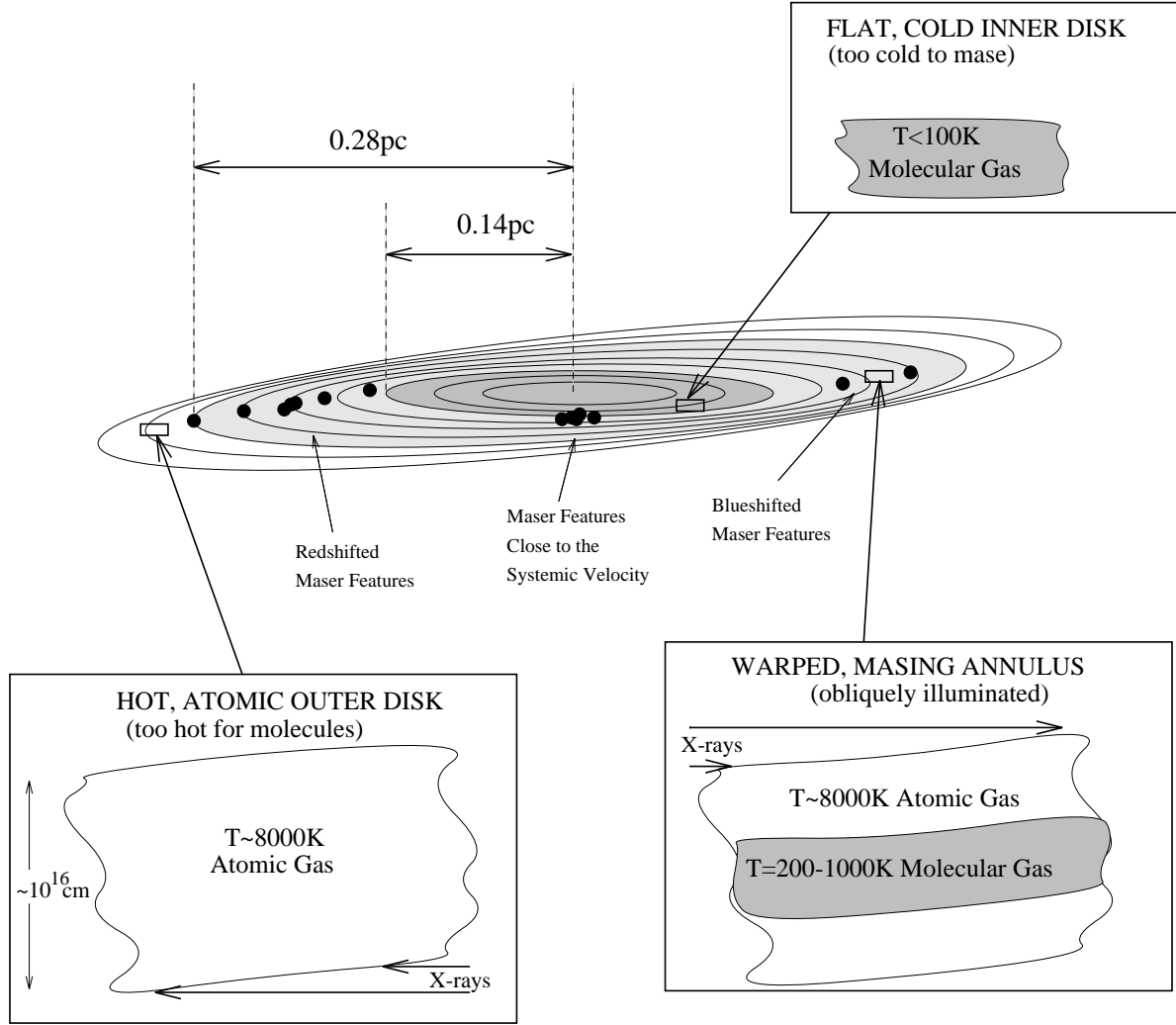


Figure 6: Structure of the accretion disk in NGC 4258, as inferred from observations of water maser emission. The disk temperature within the masing region is set by the X-ray heating rate; the outer edge is determined by the disk pressure (where it undergoes a phase transition from partly molecular to completely atomic) and the inner edge results from the flattening of the disk warp, so that it is no longer irradiated by the central source. From Neufeld & Maloney (1995).

emission in NGC 4258 is due to shocks in spiral density waves in a self-gravitating disk⁵. The main motivation for this was the hint of “regular” spacing in radius and velocity of the high-velocity features in the disk, as seen in the data of Miyoshi et al. (1995) (see Figures 4b and c). Although this model contains some *ad hoc* assumptions (e.g., it is assumed that conditions in the disk are such that water maser action will occur when a density wave – which by fiat produces a shock of the required speed – passes through the disk between 0.14 and 0.28 pc, and nowhere else; also, all of the predicted maser luminosities are scaled to a disk thickness of 10^{16} cm, an order of magnitude larger than the observed upper limit to the dimensions of the maser spots), it did make very definite predictions about the pattern of accelerations that should be seen as a function of impact parameter. This model also explained the relative weakness of the blue-shifted high-velocity features relative to the red-shifted features as a consequence of absorption by non-masing water. Indeed, Maoz & McKee made a generic prediction that all such disks should exhibit the same blue/red asymmetries, since this is an intrinsic feature of the spiral shock model. The mass accretion rate in this model is approximately two orders of magnitude larger than the rate inferred by NM95.

The predicted acceleration pattern was tested by Bragg et al. (2001), who found no evidence to support the MM98 model, for any chosen pitch angle of the spiral pattern. The key point is that in the MM98 model, all of the blue-shifted features should exhibit positive accelerations and the red-shifted negative, but in fact positive and negative \dot{v} are seen for both sides. Furthermore, both NGC 3079 (Nakai et al. 1995) and NGC 5793 (Hagiwara et al. 1997) have exhibited blue-shifted emission that is stronger than the red-shifted emission (always, in the case of NGC 3079), while the high-velocity emission features in IC 2560 are nearly symmetric in intensity (Ishihara et al. 2001). Hence at present there is no reason to suppose that this model applies to NGC 4258, or any other megamaser source.

Desch, Wallin, & Watson (1998) proposed that rather than X-ray irradiation, the maser emission in NGC 4258 is powered by viscous dissipation within the accretion disk itself. This requires that the energy generated by viscous dissipation is deposited in a manner which is not proportional to the local density. The viscous heating rate per unit disk face area is

$$D(R) = \frac{3GM\dot{M}}{8\pi R^3} \quad (7)$$

while the disk surface density

$$\Sigma(R) = \frac{\dot{M}}{3\pi\nu} \quad (8)$$

where the radial dependence of Σ is contained entirely in ν . Both equations (7) and (8) assume a steady-state disk far from the inner edge. Doubling equation (7) to get the total heating rate through the disk, the ratio of viscous heating rate to surface density is

$$\frac{2D(R)}{\Sigma(R)} = \frac{9}{4} \frac{GM\nu}{R^3} \quad (9)$$

⁵Note that in any scenario in which the maser emission arises in a disk, we must always view it close to edge-on if we are to see the maser emission, which will be strongly beamed in the disk plane.

which is *independent* of \dot{M} . This is also the vertically-averaged heating rate per particle, which, again assuming the α -prescription for viscosity and a thin, Keplerian disk, as above, can be written as

$$\frac{\bar{\Gamma}(R)}{\bar{n}_{\text{H}_2}(R)} = 2.1 \times 10^{-24} \frac{\alpha M_8^{1/2} c_1^2}{R_{\text{pc}}^{3/2}} \text{ erg s}^{-1} \quad (10)$$

where $\bar{\Gamma}(R)$ is the vertically-averaged heating rate per unit volume and \bar{n}_{H_2} is the similarly averaged number density of molecular hydrogen; c_1 is the gas sound speed in units of 1 km s^{-1} (appropriate for molecular gas at a few hundred K). Note that this value of the viscous heating rate per particle is independent of how $\bar{\Gamma}$ and \bar{n}_{H_2} are calculated from D and N_{H_2} , respectively, provided only that they are calculated the same way. Plugging in the numbers appropriate to NGC 4258,

$$\frac{\bar{\Gamma}}{\bar{n}_{\text{H}_2}} = 3.8 \times 10^{-23} \alpha \text{ erg s}^{-1}. \quad (11)$$

For $\alpha \lesssim 1$, this is approximately two orders of magnitude smaller than the heating rate per particle needed to power H_2O maser action in the disk (Desch et al. 1998). Hence it is necessary to assume that the viscous energy is deposited in a different fashion with height z than the gas density $\rho(z)$, a not implausible assumption.

The simplest assumption (and one that is in reasonable agreement with the results of Stone et al. 1996, who explicitly calculated the energy deposition as a function of height in three-dimensional magnetohydrodynamic simulations of the magnetorotational instability) is to assume that the viscous heating rate per unit volume is independent of z . In this case the heating rate per particle simply increases with height as a Gaussian with scale height equal to the gas scale height H ; the ratio of the heating rate per particle to the vertically-averaged heating rate per particle derived above (equation 9 or 10) is

$$\frac{\Gamma/n(z)}{\bar{\Gamma}/\bar{n}} \simeq \exp(z^2/2H^2) \quad (12)$$

which is (not surprisingly) independent of everything except the height above the disk midplane in scale heights. In particular, this is independent of \dot{M} ; it is just the ratio of the midplane density to the density at height z .

To maintain high enough temperatures to power the maser emission, we require a local heating rate which exceeds the vertically-averaged rate by a factor of about $100/\alpha$. Thus it is necessary that

$$\exp(z^2/2H^2) \approx 100/\alpha \quad \implies \quad \frac{z}{H} \gtrsim 3, \quad (13)$$

even for $\alpha \approx 1$, *i.e.*, the density must drop to $1/100$ of the midplane value. The only constraints on \dot{M} are then:

- (a) The densities three or more scale heights above the plane must be high enough to excite the masing transitions;

(b) The column density of masing gas must be large enough to be detectable.

This can be made to work for NGC 4258, for values of \dot{M}/α comparable to (or larger than) the NM95 rate, in the sense that the above conditions can be satisfied. While the outer edge can be understood as the result of either the gas density or column density declining below the threshold for maser emission, the inner radial cutoff is unexplained, since the warping of the disk is irrelevant, and the masing layer should simply move higher into the disk atmosphere with decreasing radius. However, it appears very unlikely that this mechanism can apply to the other masing disk systems that have been observed (see section 4). In general, the factor by which the local viscous heating rate (in the masing region) has to exceed the vertically-averaged rate is

$$\frac{\Gamma/n(z)}{\bar{\Gamma}/\bar{n}} \sim 1300 \frac{R_{\text{pc}}^{3/2}}{\alpha M_8^{1/2}}. \quad (14)$$

For NGC 1068, for example, with $R_{\text{pc}} \sim 0.65$, $M_8 \sim 0.15$, this is a factor of $\sim 1800/\alpha$. For the other systems that appear to be disk-like (Moran et al. 1999; §4) the spatial scales are also typically $r_{\text{maser}} \sim 1$ pc, while the masses of the central objects are five to ten times smaller than in NGC 4258 or NGC 1068. This leads to prohibitively large values of \dot{M}/α , e.g., in excess of $2 M_\odot \text{ yr}^{-1}$ for the maser disk in NGC 1068. This is inconsistent with the mass and luminosity of the central source in NGC 1068 (which, radiating at nearly Eddington luminosity, is most definitely *not* an ADAF: see below), unless $\alpha \sim 10^{-2}$. However, since the value by which the local heating rate must exceed the vertically-averaged value itself scales as α^{-1} (equation 14), the discrepancy cannot be solved this way, since the values of \dot{M}/α required to satisfy the density or column density requirements will simply scale up proportionately as α is decreased. Hence I am rather skeptical about the viability of this mechanism as a general explanation for water maser emission in AGN⁶.

Kartje, Königl, & Elitzur (1999) proposed a variant X-ray powered accretion disk model, which differs from NM95 in (a) being specifically clumpy (although the NM95 model is referred to throughout as the “homogeneous disk model”, as though this is a requirement, the same arguments carry over to a clumpy disk, the only difference being that the critical pressure refers to the clumps containing the bulk of the mass at a given radius); (b) has the clumps in NGC 4258 occur in a disk-driven hydromagnetic

⁶There is an additional aspect of this model that is rather problematic for high accretion rates. As noted earlier, a fundamental requirement for maser action is departure from thermodynamic equilibrium, in particular, that the gas temperature exceed the temperature of the radiation field in the mid- to far-IR. Desch et al. calculated the temperatures in their model under the assumption that the dust temperature is determined by the continuum emission of the central source incident on the disk, while the gas temperature is determined by viscous heating, and conclude that T_{gas} can exceed T_{dust} by a large enough factor to allow maser emission. This may be plausible for the NM95 mass accretion rate, since in this case the disk is not very optically thick (at least in the masing region) in a Rosseland mean sense, and the local viscous heating is substantially smaller than the incident continuum. For accretion rates that are much larger than this, however, neither of these statements are true, and it is difficult to see why the dust and gas temperatures will not be well coupled in a disk heated dominantly by viscous heating.

wind: the disk itself is actually flat, not warped; and (c) has a mass accretion rate that is two orders of magnitude higher than that derived by NM95, similar to MM98. One might perhaps be somewhat surprised that the observed disk should appear so thin, warped, and Keplerian if the emission actually arises in clumps uplifted off the flat disk in a wind.

Since the NGC 4258 portion of this model has parameters that have of course been chosen to match the observations, perhaps its most direct prediction is that the mass accretion rate is much larger than inferred by NM95, exceeding $\dot{M} \approx 10^{-2} M_{\odot} \text{yr}^{-1}$. This is also true of the MM98 model, since accretion rates much higher than the NM95 rate are required to make the disk self-gravitating, and high mass accretion rates were also favored by Desch et al. (1998). Since the luminosity of the nucleus of NGC 4258 is well determined observationally (Makishima et al. 1994), all of these high mass accretion rate models require that the inner portion of the accretion disk (assuming steady accretion; I will return to this point shortly) radiates very inefficiently. Hence these papers have all appealed to “ADAF” models (for Advection-Dominated Accretion Flow; this is really just a renaming of what used to be referred to as “ion tori” [See Svensson 1999]) for accretion, in which the inner region of the flow is very hot (with the ions at close to the virial temperature), but radiates very inefficiently, as the electrons are not well coupled to the protons (so that $T_e \ll T_i$) (Ichimaru 1977; Rees et al. 1982; Phinney 1983; the modern incarnations begin with Narayan & Yi 1994 and Abramowicz et al. 1995, with literally dozens of follow-up papers). These flows exist only for values of \dot{M} below a critical threshold; for higher \dot{M} only the standard thin, “cold” (i.e., $T \ll T_{\text{vir}}$) disk solutions exist.

Indeed, given the extremely low fractional Eddington luminosity of NGC 4258, there were immediate attempts to fit it into the ADAF framework (Lasota et al. 1996), since if its accretion is not described by an ADAF, there is really no reason to assume that ADAF models apply to any AGN. (As noted above, the fractional Eddington luminosity for NGC 1068 is so high – nearly unity – that there is no question that it is *not* described by an ADAF solution.) The success of the ADAF model lies in the fits to the “spectrum” of NGC 4258 (for an example, see Figure 1 of Lasota et al. 1996). If \dot{M} is in fact much larger than the NM95 rate, we must conclude that the disk does not see the central X-ray source beyond 0.28 pc, since otherwise maser emission would arise further out, since there is no longer a transition to an atomic disk at this radius, as R_{cr} will also be much larger (see equation [4]).

At present the ADAF models for NGC 4258 have been confined to an increasingly small portion of parameter space; the absence of 22 GHz continuum emission associated with the ADAF (Herrnstein et al. 1998) and the detection of X-ray variability on timescales of $\sim 4000 - 40,000$ seconds (Fiore et al. 2001) indicate that the transition to an ADAF must occur on scales of order 100 Schwarzschild radii or less. The most definitive test for the presence of cold material close to the central black hole would be the detection of a broad Fe K α line; there has not yet been an observation of sufficient sensitivity (Reynolds, Nowak, and Maloney 2000; Fiore et al. 2001) to either detect such a line or rule one out at an interesting level.

One important point that has been raised in connection with the mass accretion

rate and the radiative efficiency is the assumption of steady-state accretion (Gammie, Blandford, & Narayan 1999). As noted earlier, the efficiency inferred by NM95 is only valid if accretion has been steady over the time it takes material to migrate from the radius of the maser disk down to the central source. However, if the disk flattens out at the inner radius of the maser disk, the viscous timescale increases by a large factor due to the drop in disk temperature, and exceeds 10^9 years. It is very unlikely that accretion has been steady on this timescale. However, viscous heating at this radius will only heat the disk to $T < 100$ K (NM95). This means that the disk will be marginally self-gravitating: the Toomre Q parameter

$$Q = \frac{3c_s^3 \alpha}{GM} \simeq 4.0 \times 10^{-3} T_3^{3/2} \frac{\alpha}{\dot{M}} \quad (15)$$

is < 1.8 for the NM95 mass accretion rate, at these low temperatures. It therefore seems plausible that the mass flow through the disk at these radii will be determined by gravitational instabilities rather than viscosity, and so the magnitude of the viscous timescale may be irrelevant.

4 Imaging 2: Is NGC 4258 Unique?

NGC 4258 was the first of the megamaser sources to be imaged with VLBI. The remarkable results obtained from this experiment generated a great deal of interest in imaging of the other H_2O megamaser sources. With existing instrumentation it is difficult to obtain VLBI observations of masers that are weaker than about 0.5 Jy because of the necessity of detecting the maser within the coherence time of the interferometer (Moran et al. 1999). By using a maser feature as phase reference, and referring the other maser features to it, it is possible to extend the coherence time, and thereby observe weaker features, but it is still a difficult endeavour (J. Moran, pers. comm.) Hence not all of the known sources can be imaged at present. To date, nine megamasers have been imaged with VLBI. Of these nine, four show strong evidence for disk structure and two show probable evidence for disks from the spatial and velocity distribution of the emission; one, for which only the systemic emission has yet been imaged, shows kinematic evidence for a disk and may be the most similar to NGC 4258 of any source yet observed. The other two sources appear to be very different in origin. Table 1 (adapted from Moran et al. 1999) summarizes the results. None of the disk sources are as well-defined as in NGC 4258, nor do any of them exhibit Keplerian rotation curves. This latter feature, at least, is not unexpected, at least in the X-ray powered maser model, as I discuss below. First I will review some of the more interesting results from the imaging studies.

4.1 NGC 1068

The archetypal Seyfert 2 galaxy NGC 1068 was the second H_2O megamaser source to be imaged with VLBI. Single-dish observations had already shown that maser emission extended up to about $\pm 300 \text{ km s}^{-1}$ away from the systemic velocity; unlike NGC 4258,

the systemic emission is not the strongest. Re-analysis of archival VLA observations by Gallimore et al. (1996) demonstrated that, in addition to the nuclear masers (i.e., the masers associated with the radio continuum emission believed to be coincident with the nucleus), a second group of fainter maser features was located about $0.3''$ (30 pc) away, at the same position angle as the radio jet. The initial VLBA observations (Greenhill et al. 1996) covered only the red and systemic velocities, and revealed a linear structure extended over about 1 parsec, oriented at 45° to the radio jet axis. Velocity gradients were suggestive of a rotating structure. Greenhill et al. suggested that this was the upper surface of an irradiated torus, and predicted that the blueshifted emission, when imaged, would form the mirror image to the redshifted. The lower (southern) half, which was missing, might be hidden by free-free absorption.

However, when the blueshifted emission was imaged, it appeared as a continuation of the redshifted emission, so that the maser emission forms one linear structure that is highly inclined to the radio jet axis. This can be fitted by a thin, rotating disk, with rotation velocities up to 330 km s^{-1} (Greenhill & Gwinn 1997). The fall-off of rotation velocity with radius is slower than Keplerian, however, declining approximately as $r^{-0.35}$. This could be due to either the mass of the disk itself, or to a central stellar cluster. There is a substantial spread of the velocities about the rotation curve, perhaps indicating a velocity dispersion of some tens of km s^{-1} . The scale of the masing region is larger than in NGC 4258, with inner and outer edges at approximately 0.65 and 1.1 pc, respectively. The enclosed mass is about $M = 1.5 \times 10^7 M_\odot$; nearly all of this must be contributed by the black hole.

The orientation of the disk with respect to the radio jet axis appears peculiar. However, Gallimore, Baum, & O’Dea (1997) imaged what appears to be a thermal source, with brightness temperatures $T_b \sim 10^5 - 10^6 \text{ K}$ between 5 and 8 GHz, that lies interior to the maser disk and is elongated perpendicular to the jet axis. This appears to be emission from the disk rather than the jet. If this is the case, then interpreting the thermal source and masing disk as one continuous structure would imply that the masing region in fact traces a severely warped disk, with a much greater inclination warp than seen in NGC 4258. Support for a disk geometry, warped or not, is also provided by the absence of accelerations of the high-velocity features: Gallimore et al. (2001) derive upper limits for the redshifted masers of $< 0.01 \text{ km s}^{-1} \text{ yr}^{-1}$ from fifteen years of monitoring data with the Effelsberg 100m telescope.

Gallimore et al. also argue that the nuclear masers vary coherently on timescales of months to years, which is much shorter than the dynamical timescale, and that therefore they must be responding to variations of the central power source. Between October and November of 1997 there was a simultaneous flare of blueshifted and redshifted maser features, which can be naturally understood as reverberation in a rotating disk. Neufeld (2000) has shown that the masers can respond to variations in the central source luminosity in two ways: increasing as the X-ray luminosity increases, which raises the maser emissivity, or decreasing as the bolometric luminosity increases, which decreases the difference between the dust and gas temperatures and therefore reduces the maser output. Either mechanism can explain the variation reported by Gallimore et al., provided that the density in the masing regions is at least $n_{\text{H}_2} \sim 10^8 \text{ cm}^{-3}$, which

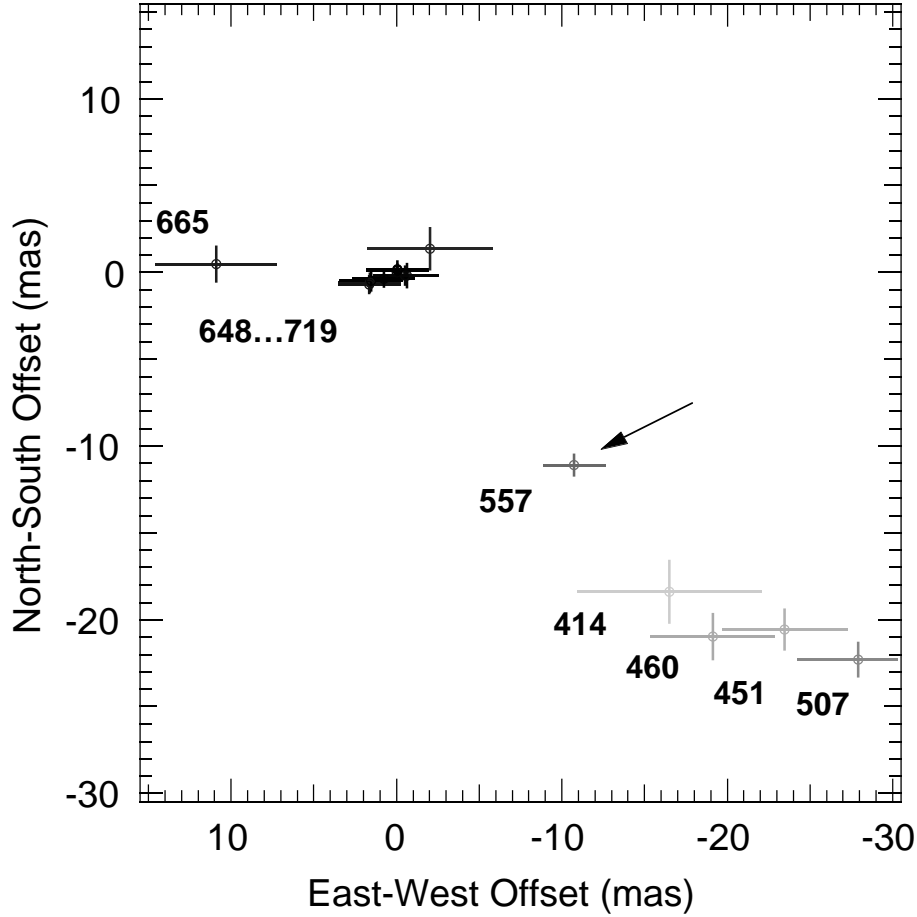


Figure 7: The spatial distribution of H_2O maser emission from NGC 4945. The labels indicate the velocities of the emission, which is also shown by the grayscale (lighter shading corresponds to bluer velocity). The arrow marks the position of the maser feature closest to the systemic velocity of the galaxy ($V_{\text{sys}} = 561 \text{ km s}^{-1}$). At the distance of NGC 4945, $1 \text{ mas} = 1.9 \times 10^{-2} \text{ pc}$. From Greenhill et al. 1997a.

is required to obtain a variability timescale as short as seen for the maser flare. Since, unfortunately, we do not have a direct view of the X-ray source in this galaxy, but see it only in reflection (as is also true for NGC 3079; see §4.3), it is not clear which mechanism is actually at work.

As noted above, NGC 1068 also possesses fainter maser emission, located approximately 30 pc away from the nucleus along the radio jet axis (Gallimore et al. 1996). Given their location, these masers may arise in a shock that arises at the interface between the radio jet and a near-nuclear molecular cloud. In support of this interpretation, the jet appears to be diverted by its interaction with the ISM at this location.

4.2 NGC 4945

The first H₂O megamaser to be discovered (dos Santos & Lepine 1979), NGC 4945 contains a luminous ($L_x \approx 6 \times 10^{42}$ erg s⁻¹) nuclear hard X-ray (1–100 keV) source (Iwasawa et al. 1993; Done, Madejski, & Smith 1996; Madejski et al. 2000), which is heavily obscured behind a column $N_H \approx 5 \times 10^{24}$ cm⁻², so that the direct X-ray emission is only observable above $E \approx 20$ keV. In fact, the obscuring column is so high that a proper treatment of the radiative transfer to take the substantial Thomson optical depth into account is necessary; this raises the hard X-ray luminosity by about an order of magnitude over simple obscuring column density models: see Madejski et al. 2000. The X-ray emission is also highly variable, with $t_{\text{var}} \sim 1$ day, implying that the sizescale of the emitting region is no more than $r \sim 10^{15}$ cm, and that the absorbing material cannot occupy a large solid angle around the disk (Madejski et al. 2000). The nuclear far-infrared luminosity is approximately an order of magnitude larger than the hard X-ray luminosity, and arises nearly entirely from a region no more than 225 pc by 170 pc in size (Brock et al. 1988).

NGC 4945 lies in the southern hemisphere ($\delta = -49^\circ$), and it is therefore very difficult to observe with the VLBA. Nevertheless, Greenhill, Moran, & Herrnstein (1997) succeeded in observing the maser emission using two of the southernmost VLBA antennas. A typical spectrum of the emission (which is time variable) is shown in Figure 1. The high velocity emission brackets the systemic emission, with velocities up to about ± 150 km s⁻¹ away from systemic; as in NGC 4258, the redshifted emission is much stronger than the blueshifted, but as in NGC 1068, the redshifted emission is also much stronger than the systemic. The spatial distribution is shown in Figure 7; note that not all of the detected emission, particularly near the systemic and blueshifted velocities, could be mapped. The structure is quite linear, tracing a shallow \mathcal{S} shape on the sky, and extends over about 40 mas (0.8 pc). The position-velocity diagram (Figure 8) bears some similarity to that of NGC 4258; however, the redshifted emission does *not* mirror the blueshifted emission, and the fall-off of velocity with impact parameter on the blueshifted side appears to be faster than Keplerian, which would imply that these features do not all lie in the plane of the sky. If one, nevertheless, interprets the emission in terms of an edge-on, rotating disk, the implied mass is $M \sim 1.4 \times 10^6 M_\odot$, and the central mass density is at least $\rho \sim 2 \times 10^7 M_\odot \text{ pc}^{-3}$. With this central mass and the observed luminosity, NGC 4945 must be radiating in excess of 10% of the Eddington limit.

4.3 NGC 3079

NGC 3079 is a relatively nearby ($D = 16$ Mpc), nearly edge-on spiral galaxy. It has a fairly high far-infrared luminosity ($L_{\text{IR}} \approx 3 \times 10^{10} L_\odot$), a LINER-type spectrum (Heckman 1980) and a spectacular nuclear outflow (see Cecil et al. 2001, and references therein), with prominent radio lobes (Duric & Sequist 1988) and loops of H α emission (Ford et al. 1986) extending a kpc or more away from the nucleus along the minor axis. NGC 3079 also has a prominent ring of molecular material, seen in CO emission, extending from approximately 250 to 750 pc, and a very compact, luminous CO peak

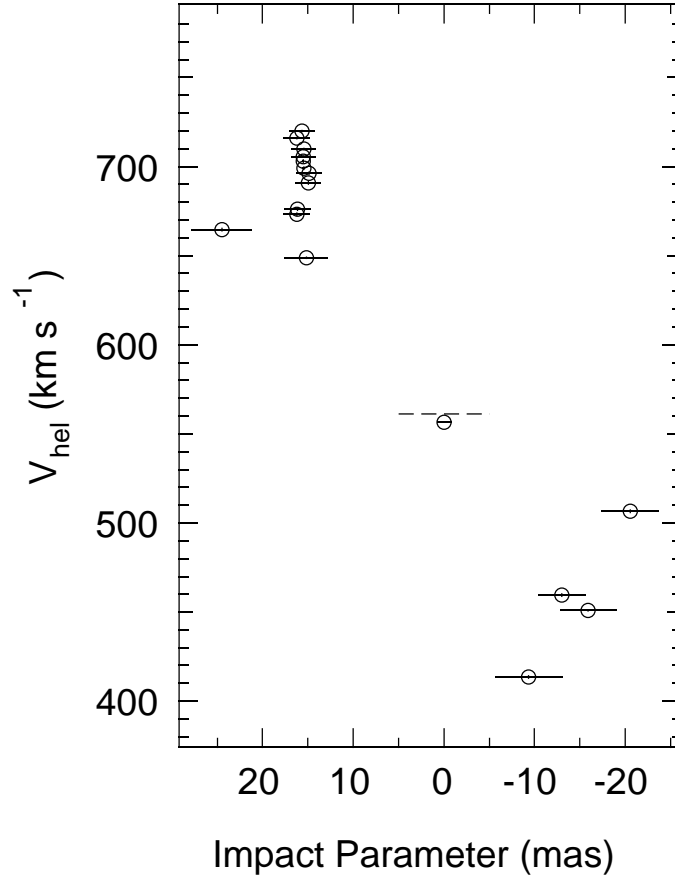


Figure 8: The velocities of the mapped maser features in NGC 4945 as a function of impact parameter. The positions are measured relative to the feature that is closest in velocity to the systemic velocity (dashed line). The error bars on position are 3σ . From Greenhill et al. 1997.

centered on the nucleus (Sofue et al. 2001, and references therein).

NGC 3079 possesses one of the most luminous H₂O megamasers known (Henkel et al. 1984a,b; Haschick & Baan 1985). The maser emission is almost entirely concentrated to velocities blueward of the systemic velocity, and it is strongly variable in flux density and line width, the flux density having varied by about a factor of eight over ten years, while the linewidths have fluctuated by up to a factor of two (Baan & Haschick 1996).

The maser emission from NGC 3079 was observed using the VLBA by Trotter et al. (1998). The observed distribution of maser emission on the sky, color-coded according to velocity, is shown in Figure 9. The two dashed lines show the major axis of the molecular disk discussed above (the nearly vertical line) and the axis of the nuclear jet. The emission arises in compact clumps, with sizes $\lesssim 0.02$ pc; most of the emission arises in a region less than 0.2 pc in diameter, spread over a velocity range of about 130 km s⁻¹. The size of the circles representing the maser emission are proportional to the logarithm of the flux density, and they are labeled with the velocity of the approximate flux density peak. The inset in Figure 9 (from Trotter et al.) shows an expanded version of the concentrated emission; this region includes the maser peak, at $v_{\text{LSR}} = 957$ km s⁻¹. Also sketched in Figure 9 are the positions and approximate sizes of 22 GHz continuum features.

It is evident from Figure 9 that the maser emission from NGC 3079 differs markedly from the distribution seen in NGC 4258. The maser spots are approximately aligned with the larger-scale molecular disk, and their measured Doppler velocities are consistent with rotation in the same sense as the molecular disk. However, there is evidently a large nonrotational component to the velocity field: as noted above, the spread in velocities within the compact grouping of maser spots covers the entire range of blueshifted emission. This may indicate large turbulent velocities in the disk. The 22 GHz continuum emission is dominated by an unresolved ($\lesssim 0.1$ pc) source (labeled B in Figure 9) that lies approximately 0.5 pc to the west of the maser peak. There is no maser emission associated with this (or any other) continuum peak; this argues against the suggestion that the unusually luminous maser emission in NGC 3079 is the result of beamed, unsaturated amplification of compact continuum emission by foreground molecular gas.

A sketch showing the model of the emission suggested by Trotter et al. (1998) is shown in Figure 10; this must be regarded as highly speculative (see below). As with NGC 4945, the emission has been interpreted within the framework established by NGC 4258, i.e., as a rotating disk, seen close to edge-on. The disk thickness is unknown. Trotter et al. argued that the maser emission could not be powered by X-ray irradiation, as the observed X-ray luminosity of NGC 3079 was only $L_x \sim 10^{40}$ erg s⁻¹ in soft X-rays, and there was no indication of a nuclear hard X-ray source. However, *BeppoSax* observations (Iyomoto et al. 2001) show that, as in the case of NGC 4945, there is a luminous ($L_x \sim 10^{42} - 10^{43}$ erg s⁻¹) hard X-ray source buried beneath Compton-thick absorption, thus eliminating this argument. The overall distribution of velocities is consistent with the presence of a binding mass $M \sim 10^6 M_\odot$ within 0.5 pc. If this is indicative of the central mass, the hard X-ray luminosity indicates that the AGN contributes a large fraction of the far-infrared luminosity of the nucleus of NGC 3079,

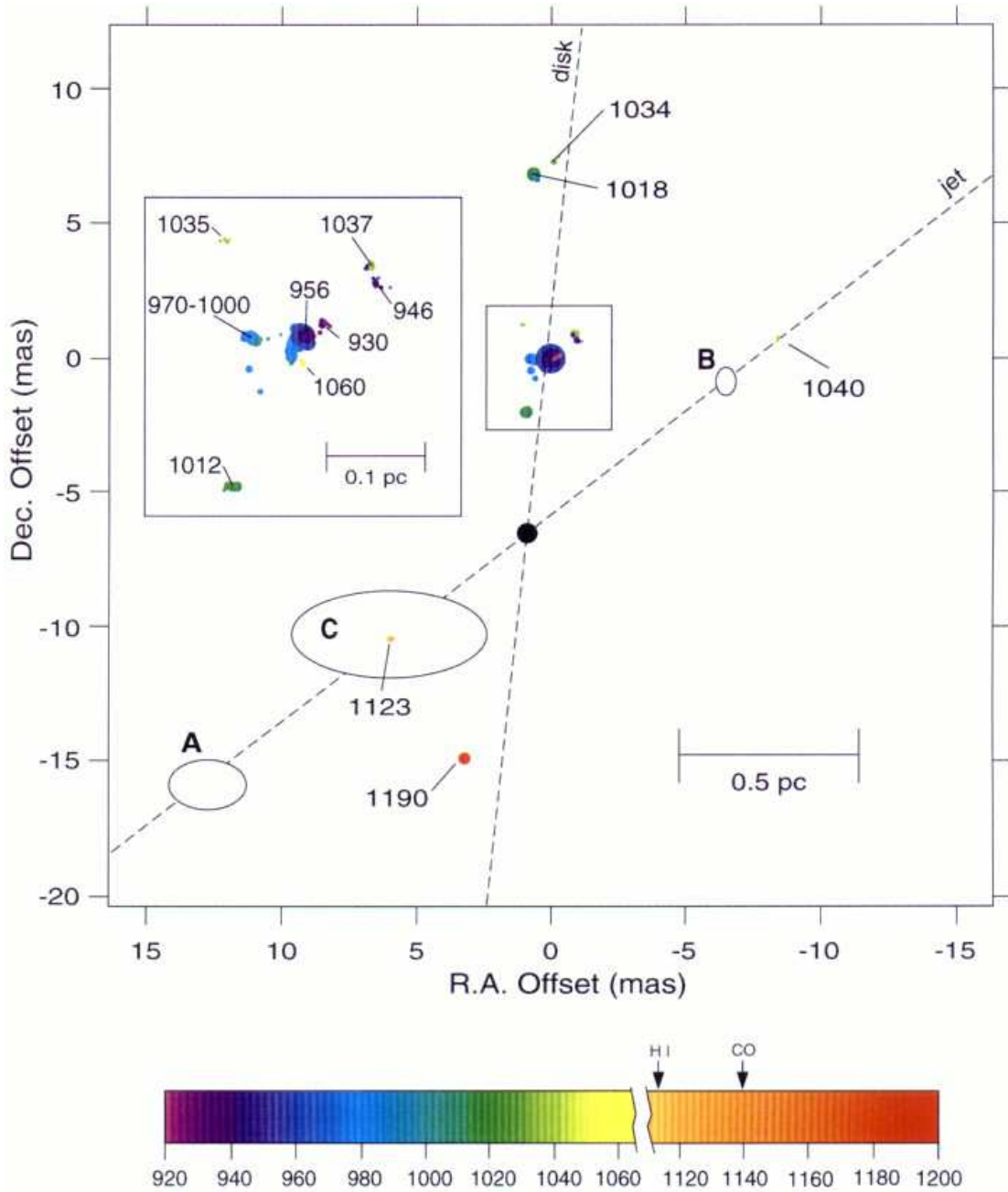


Figure 9: The spatial and velocity distribution of the maser emission in NGC 3079, as observed with the VLBA, from Trotter et al. (1998). The spots marking the maser features are sized according to the logarithm of the flux density and color-coded according to velocity; the labels show the velocity of the approximate flux density peak. Also sketched in are the approximate positions and sizes of 22 GHz radio continuum features, and the axes of the large-scale molecular disk and the nuclear radio jet.

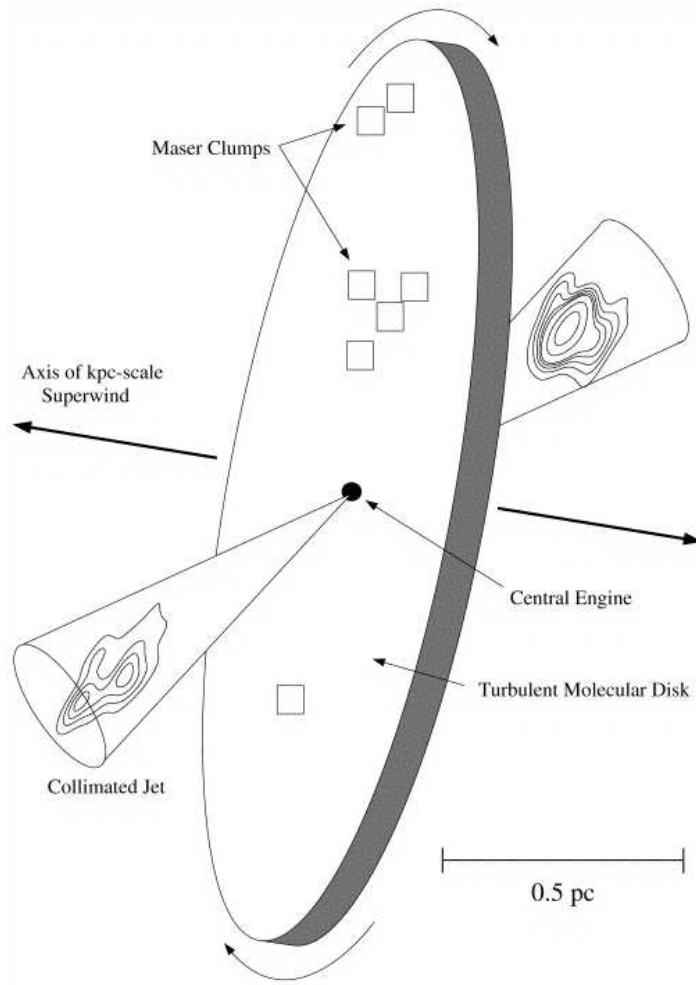


Figure 10: Model of the central pc of NGC 3079, based on VLBA observations (from Trotter et al. 1998). The maser spots are distributed in a disk that is close to edge-on; the disk center is assumed to be near where the major axis of the maser emission and the jet axis intersect.

and it is radiating at 1 – 10% of the Eddington limit.

Sawada-Satoh et al. (2000) argue that this interpretation is not correct, as they identify the bright continuum source (labeled “B” in Figure 9) as the location of the nucleus. This identification is based on the apparent fixed position of component B with respect to the strongest maser feature based on several years of observations, unlike components A and C, which they argue are probably jet features. Sawada-Satoh et al. suggest that the maser emission arises in a geometrically thick structure whose rotation axis passes through component B; this axis is inclined by about 110° to the large-scale rotation axis of the galaxy.

4.4 Circinus

The Circinus galaxy is a nearby ($D = 4$ Mpc) Seyfert 2 galaxy in the Southern hemisphere, and was one of the first megamaser sources to be discovered (Gardner & Whiteoak 1982). It bears interesting similarities to several of the galaxies discussed above, including the presence of a luminous ($L_x \sim 10^{42}$ erg s $^{-1}$) hard X-ray source hidden behind Compton-thick obscuration (Matt et al. 1999), a nuclear outflow along the minor axis (seen in bipolar radio lobes: Elmouttie et al. 1998), a broad (opening angle $\sim 90^\circ$) ionization cone (Marconi et al. 1994; Veilleux & Bland-Hawthorn 1997) and a nuclear (\sim several hundred pc) molecular ring seen in CO emission (Curran et al. 1998). The maser spectrum shows emission out to approximately ± 200 km s $^{-1}$ with respect to the systemic velocity; the red-shifted emission is stronger than the blue, and both are substantially stronger than the systemic (Nakai et al. 1995; Braatz, Wilson, & Henkel 1996; Greenhill et al. 2001). The maser emission is highly variable, and the spectrum alters substantially on timescales of order one month (Whiteoak & Gardner 1986). Variability has been seen on timescales as short as a few minutes (Greenhill et al. 1997b), much more rapidly than any other source. This rapid variability is almost certainly the result of interstellar scintillation; Circinus lies at low Galactic latitude, $b = -3.8^\circ$.

VLBI observations of the H $_2$ O maser emission from Circinus have been reported by Greenhill (2001b) and Greenhill et al. (2001). The emission was observed using the Australia Telescope Long Baseline Array in 1997 and 1998. The distribution on the sky (with gray scale indicating velocity) is shown in Figure 11. Although this appears somewhat confusing, when combined with the velocity information (Figure 12) a coherent picture emerges. At each observing epoch, the maser emission consists of three components: a thin, shallow \mathcal{S} shape on the sky (similar to NGC 4945), comprised of highly redshifted and blueshifted emission; emission at close to the systemic velocity, which lies between the two arcs of high-velocity emission; and modestly Doppler-shifted (up to ~ 100 km s $^{-1}$) emission whose spatial distribution is correlated with the sign of the velocity shift: blueshifted emission on the southeast side, redshifted on the northwest side.

The high-velocity and near-systemic velocity emission can be fitted by a thin (thickness < 2 mas = 0.04 pc), warped disk, viewed edge-on, with an outer radius of approximately 0.4 pc (20 mas) and an inner edge at ~ 0.1 pc. The orbital velocity (assuming circular motion) at the inner edge is 237 km s $^{-1}$, giving an enclosed mass $M \simeq 1.3 \times 10^6 M_\odot$, and a minimum mass density $\rho \sim 3 \times 10^8 M_\odot$ pc $^{-3}$. With this central mass, the observed X-ray luminosity implies a fractional Eddington luminosity of order 10%. The high-velocity emission on the redshifted side can be fitted with a peak velocity that declines with impact parameter b approximately as $b^{-0.4 \pm 0.05}$. The fact that the rotation curve is shallower than Keplerian could be due to the mass of the disk; this would imply a disk mass $\sim 10^5 M_\odot$ between 0.1 and 0.4 pc. Alternatively, this could be due to the contribution of a central stellar cluster. Lending additional support to this model is the fact that a single position-velocity gradient connects the highest velocity red- and blue-shifted emission, and the near-systemic velocity emis-

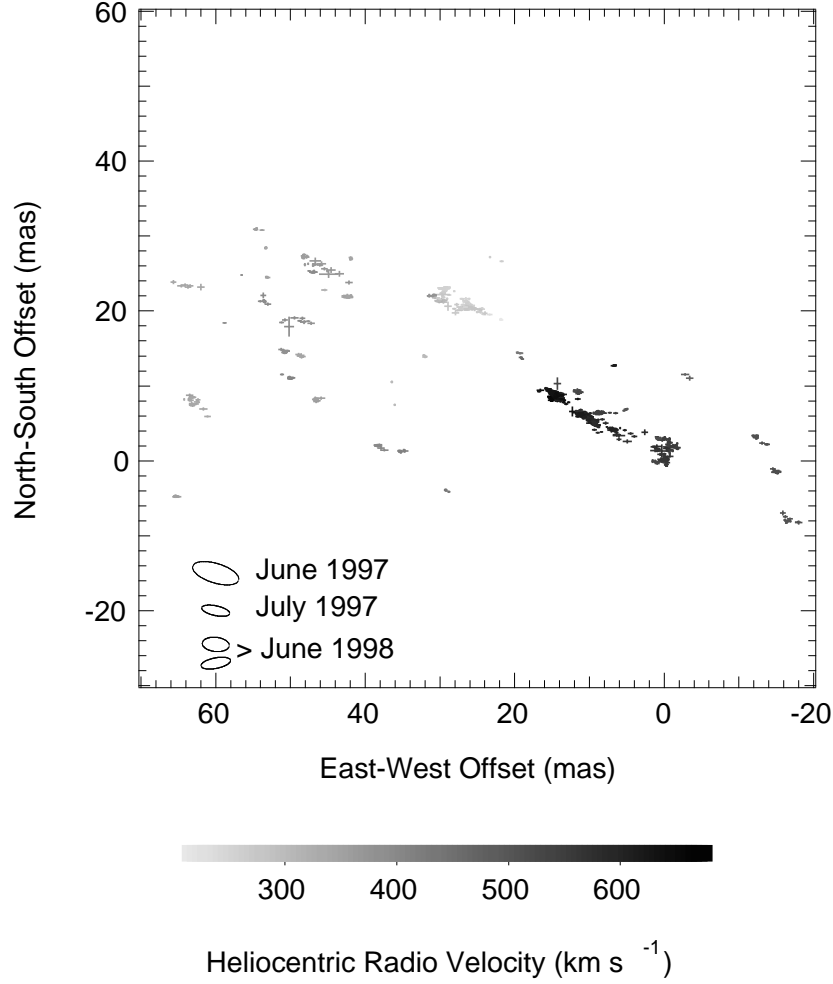


Figure 11: The spatial distribution of H_2O maser emission from the Circinus galaxy. The observations were actually taken at three separate epochs; the synthesized beam sizes are plotted at lower left. The velocity of the emission is indicated by the gray scale. At the distance of Circinus, $1 \text{ mas} = 1.9 \times 10^{-2} \text{ pc}$. The systemic velocity $V_{\text{sys}} \simeq 440 \text{ km s}^{-1}$. From Greenhill et al. (2001).

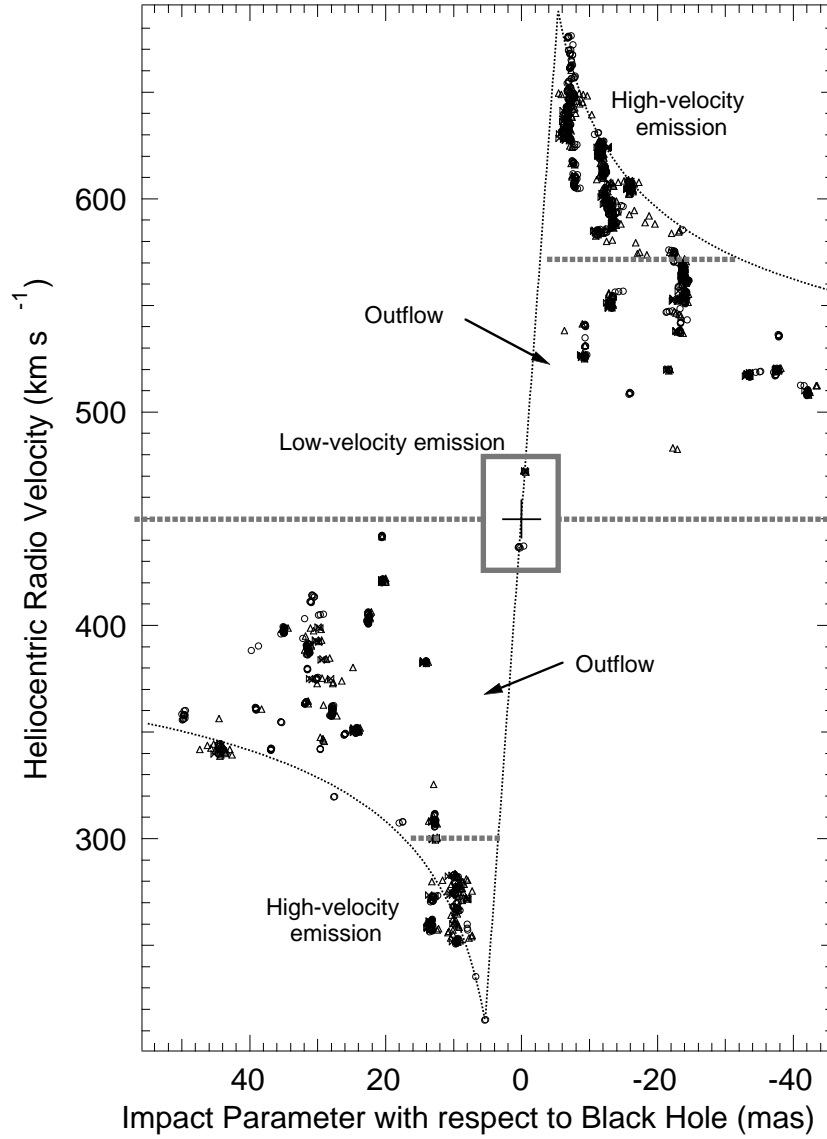


Figure 12: Position-velocity diagram for the Circinus maser emission. Labels indicate features of the model discussed in the text. The rotation curve declines with impact parameter b approximately as $b^{-0.4 \pm 0.05}$. From Greenhill (2001b).

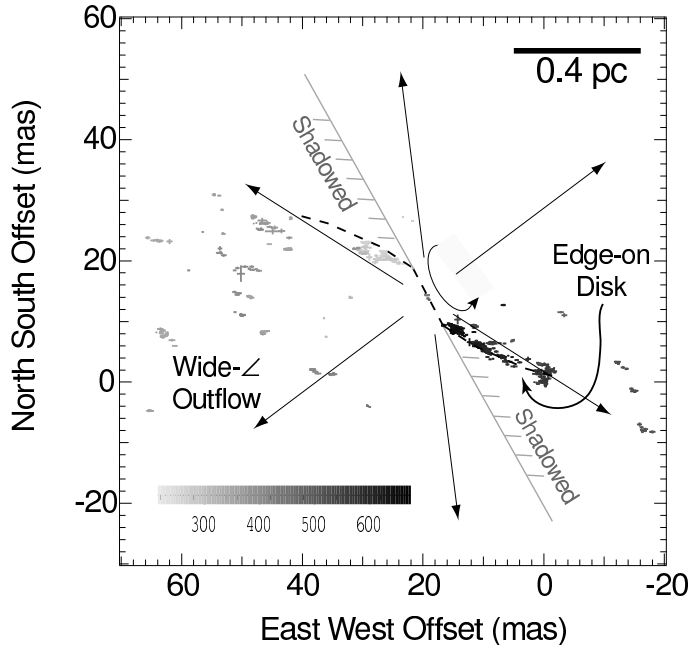


Figure 13: Model of the warped accretion disk and outflow structure in the Circinus galaxy, superimposed on the spatial distribution of the emission. From Greenhill (2001b).

sion; this is also seen in NGC 4258, and is expected if all of the near-systemic emission arises at the inner radius of the disk (although this emission is relatively much weaker than in NGC 4258).

What does the intermediate-velocity gas represent? Greenhill (2001b) and Greenhill et al. (2001) interpret this as a fairly broad-angle outflow (see Figure 13). The systematic redshifting and blueshifting with position on the sky indicate that the outflow is tipped with respect to our line of sight. The high-velocity emission ceases where it would be intersected by the outflow, which may indicate that the disk is broken up by the interaction. Interestingly, all of the outflow maser emission arises in regions where the view of the central source would not be shadowed by the disk, which suggests that the maser emission is due to irradiation of the outflow by hard X-rays from the central source. Furthermore, the edges of the shadowed zone coincide very well with the boundaries of the kiloparsec-scale ionization cone seen to the west of the nucleus. However, truncation of the disk also implies that the central black hole will be starved by exhaustion of the disk mass in no more than $\sim 10^7$ years (Greenhill 2001b).

4.5 IC 2560

IC 2560 is a southern ($\delta \approx -33^\circ$) barred spiral in the Antlia cluster, at a distance of 26 Mpc. It is classified as a Seyfert 2 on the basis of optical spectra (Fairall 1986). H_2O maser emission was first detected by Braatz et al. (1996); the emission velocity was close to the systemic velocity of the galaxy.

The maser emission was reobserved by Ishihara et al. (2001), using both single-dish

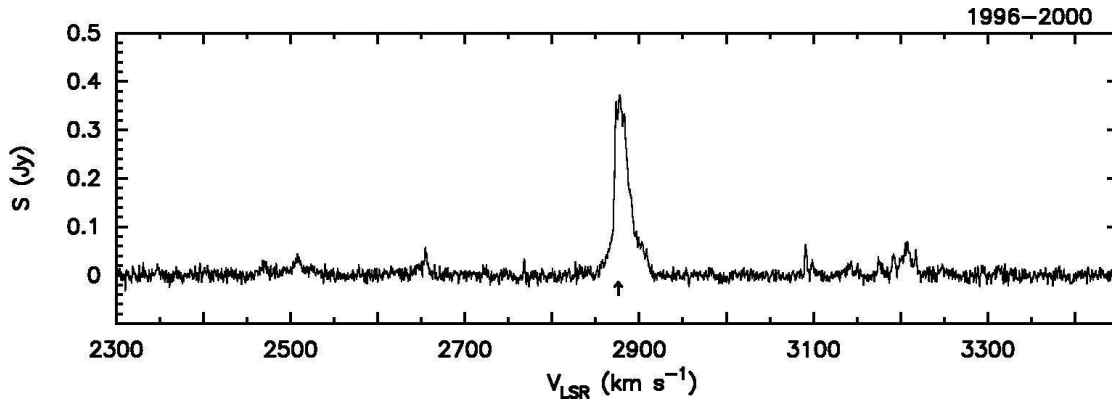


Figure 14: Spectrum of the H₂O maser emission from IC 2560 obtained with the NRO 45m telescope, averaged over all epochs. The arrow marks the systemic velocity of the galaxy. From Ishihara et al. (2001).

telescopes (the NRO 45m and the Parkes 64m dishes) and the VLBA. Multiple epochs were obtained, with observations spanning the period 1996–2000. Most of the flux is contained in the emission around the systemic velocity, which consists of a number of narrow individual features blended together over a band $\Delta V \approx 60 \text{ km s}^{-1}$ wide. (This was the only emission detected by Braatz et al.) The peak flux density is variable and has reached a maximum of about twice the value at the time of the Braatz et al. observation. Most interestingly, however, is the detection of additional, high-velocity emission, extending to approximately 400 km s^{-1} away from V_{sys} to both the red and the blue (see Figure 14). The redshifted emission is only slightly stronger than the blueshifted; the brightest high-velocity emission features are about 12 – 14% of the peak flux density.

The spectrum of IC 2560 bears remarkable similarity to that of NGC 4258 (compare Figure 14 with the top panel of Figure 4), in that there are weaker, high-velocity features spread over a substantial range to either side of the systemic emission, although the velocities are not as high in IC 2560, and the high-velocity emission is more symmetrically distributed than in NGC 4258. This is the only megamaser observed to date other than NGC 4258 in which the systemic velocity emission is much stronger than the high-velocity emission. This is not the only similarity, however. Ishihara et al. claim that over the course of the monitoring period (4.4 years using the NRO 45m and 1.1 year with the Parkes 64m), the systemic velocity features showed a secular drift to redward, at a rate $\dot{v} \simeq 2.6 \text{ km s}^{-1}\text{yr}^{-1}$. In NGC 4258 this drift (at $\dot{v} \simeq 9 \text{ km s}^{-1}\text{yr}^{-1}$) is interpreted as centripetal acceleration, as discussed in §3. A similar velocity drift has been seen in NGC 2639 (Wilson et al. 1995), with $\dot{v} \simeq 6.6 \text{ km s}^{-1}\text{yr}^{-1}$. One high-velocity feature was also monitored over a period of about a year and showed no secular acceleration, with an upper limit $\dot{v} \lesssim 0.5 \text{ km s}^{-1}\text{yr}^{-1}$.

Given the spectral similarities, one might expect imaging of the maser emission to be equally intriguing. Unfortunately, only the systemic velocity emission has been observed with VLBI so far, as the high-velocity emission had not been detected at

the time of the VLBA observation. Furthermore, the high-velocity emission is faint, with flux densities $\sim 0.050.1$ Jy, so that imaging this emission will be very difficult. Nevertheless, the results are indeed interesting. Figure 15 (from Ishihara et al. 2001) shows the spatial distribution of the emission and position-velocity cuts in both right ascension and declination. The emission is confined to a region approximately 0.1 mas by 0.2 mas in RA and Dec (0.01×0.02 pc at 26 Mpc); note that the position errors in declination are much larger than those in RA. This is similar to the spatial extent of the systemic velocity emission in NGC 4258. Furthermore, the position-velocity diagram in RA shows a systematic, linear trend, as in NGC 4258, with a magnitude $dv/db \simeq 0.85 \pm 0.27$ km s $^{-1}$ μ as $^{-1}$. (No trend is seen in the p-v diagram in Dec, which may be due to the large position errors or to the orientation.) There is also an unresolved continuum source detected at 22 GHz, with a very high brightness temperature ($T_b \gtrsim 3 \times 10^{11}$ K), which is coincident with the grouping of maser emission within the errors.

The maser emission in IC 2560 is certainly suggestive, although the rotation curve has not yet been obtained. When placed in the framework of an edge-on, Keplerian disk, the observations imply a disk with inner and outer radii of 0.07 and 0.26 pc, respectively, in orbit around a central mass of $M = 2.8 \times 10^6 M_\odot$, about an order of magnitude smaller than that for NGC 4258 or NGC 1068, but comparable to the central masses inferred for NGC 4945, Circinus, and NGC 3079⁷. It must be admitted that the distribution of systemic emission on the sky does not appear disk-like. However, it must also be remembered that IC 2560 is about 3.5 times further away than NGC 4258, so that (along with the smaller inner radius) the angular scale of the emission is smaller by about a factor of six. Furthermore, the emission is several times weaker than in NGC 4258, so that the positional error bars are quite large, especially in declination, where they are 50 – 60 μ as.

With a maximum rotation velocity of 418 km s $^{-1}$, the velocity drift of the systemic velocity features places them at 0.07 pc, which Ishihara et al. identify with the inner radius of the disk. If this is correct, the lower limit to the central mass density is $\rho \gtrsim 2.1 \times 10^9 M_\odot$ pc $^{-3}$, second only to NGC 4258 among the maser disks observed to date. As in NGC 4258, this location for the systemic velocity features is also supported by the gradient seen in the position-velocity diagram: for a given enclosed mass M , the radius implied for a measured dv/db (where v is the projected velocity and b is the impact parameter), for a Keplerian rotation curve, is

$$R = \left[\frac{(GM)^{1/2}}{dv/db} \right]^{2/3} = 4.66 \times 10^{-3} \frac{M_6^{1/3} d_{\text{Mpc}}^{2/3}}{(dv/db)^{2/3}} \text{ pc} \quad (16)$$

where M_6 is the mass of the central black hole in units of $10^6 M_\odot$, d_{Mpc} is the distance to the host galaxy in Mpc, and the velocity gradient dv/db is in km s $^{-1}$ μ as $^{-1}$. For IC 2560, equation (16) yields $R = 0.064 \pm 0.02$ pc, in excellent agreement with the value estimated from \dot{v} . This agreement also implies that the disk major axis is aligned

⁷With this mass, the inner radius of the maser disk is at $R \simeq 2.6 \times 10^5$ Schwarzschild radii, while the outer edge lies at nearly $10^6 R_s$.

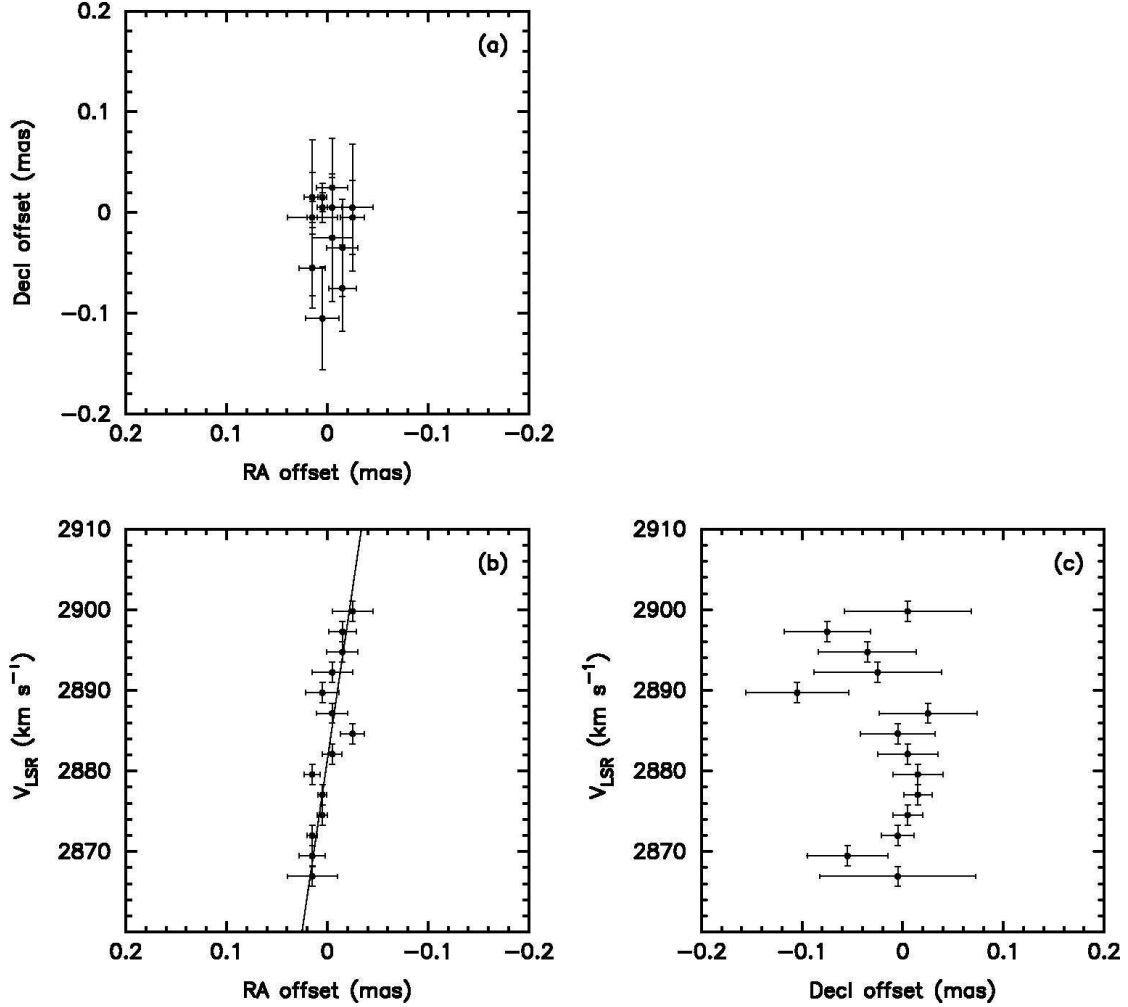


Figure 15: Spatial and velocity distribution of the systemic-velocity maser emission from IC 2560. (a) shows the position of the maser emission on the sky. (b) and (c) show position-velocity diagrams for cuts in right ascension and declination, respectively. The RA p-v cut shows clear evidence for a systematic, linear gradient of velocity with impact parameter. From Ishihara et al. (2001).

within $\sim 20^\circ$ of east-west. The velocity extent of the systemic emission implies (in the Keplerian disk framework) a very similar beaming angle to NGC 4258, about 9° .

There is one additional similarity between IC 2560 and NGC 1068. Ishihara et al. (2001) analyzed the X-ray emission from IC 2560, which was observed by *ASCA* in 1996 for approximately 42 ksec with the GIS and SIS spectrometers. Although the S/N is poor, Ishihara et al. find evidence for a heavily-absorbed ($N_H \sim 3 \times 10^{23} \text{ cm}^{-2}$) hard X-ray source, with a 2–10 keV X-ray luminosity $L_x \sim 10^{41} \text{ erg s}^{-1}$. It could be substantially lower than this; a much higher S/N spectrum is needed. Assuming that this represents 10% of the bolometric luminosity, the fractional Eddington luminosity is of order 10^{-3} , which classes IC 2560 with NGC 4258 as having very low L/L_{Edd} , as opposed to the other possible maser disk systems with $L/L_{\text{Edd}} \sim 0.1$ or greater. If we make the assumption that the maser emission is distributed in a thin, Keplerian disk that is irradiated by the central X-ray source, as in NGC 4258, and apply the theory of NMC to identify the outer edge of the disk with the molecular-to-atomic phase transition (equation 4), we obtain a mass accretion rate $\dot{M}/\alpha \sim 8 \times 10^{-4} M_\odot \text{ yr}^{-1}$, and with the above estimate of the luminosity, a radiative efficiency $\epsilon \sim 0.02/\alpha$, indicating that the luminosity of IC 2560 is low simply because, as in NGC 4258, the mass accretion rate is low. Further observations of this system with VLBI are eagerly awaited. If the geometry is confirmed to be similar to the NGC 4258 disk, it will be possible to obtain another purely geometric measurement of the distance to the maser disk, but for a galaxy which is nearly four times further away than NGC 4258, which would be very important for determination of H_o (as the distance determination for NGC 4258 already has been, since it allows one to simply skip over all of the argument about the distance modulus to the LMC: Newman et al. 2001).

Of the sources for which available VLBI imaging data provide evidence for maser disks, only the emission from IC 2560 appears to bear a marked similarity to the NGC 4258 disk (although until the recently discovered high-velocity emission from IC 2560 is imaged, the nature of the rotation curve will remain unknown). Is this surprising? Not necessarily, at least in one aspect.

Consider a galaxy containing a supermassive black hole in its nucleus. The black hole dominates the potential within a radius

$$R_{BH} \approx 2 \frac{M_7}{\sigma_{150}^2} \text{ pc} \quad (17)$$

where the velocity dispersion characterizing the depth of the galactic potential well (not including the contribution from the black hole) is $\sigma = 150\sigma_{150} \text{ km s}^{-1}$. Using the X-ray powered maser model of NMC and NM95, the critical radius for molecule formation can be written in terms of the fractional Eddington luminosity (cf. equation 4) as

$$R_{cr} = 1.5 \frac{(L/L_{\text{Edd}})^{0.38} M_7}{(\alpha\epsilon_{0.1})^{0.81} \mu^{0.38}} \text{ pc} \quad (18)$$

where the radiative efficiency $\epsilon = 0.1\epsilon_{0.1}$. In order for a maser disk to exhibit a

Keplerian rotation curve, it must satisfy $R_{cr} \ll R_{BH}$, or

$$\frac{L}{L_{Edd}} \ll 0.5 \frac{(\alpha\epsilon_{0.1})^{2.1} (\mu/0.25)}{\sigma_{150}^{5.3}}. \quad (19)$$

Hence only AGN with very sub-Eddington luminosities will have maser disks in the Keplerian regime. Since, as noted above, IC 2560 appears to fulfill this requirement, with $L/L_{Edd} \sim 10^{-3}$, it will be very interesting to see what VLBI reveals about the structure of the high-velocity emission.

5 Imaging 3: The Non-Disk Sources

Nearly all of the H₂O megamasers detected so far are in disk-dominated galaxies. There are two exceptions to this, which have interesting similarities to one another and also to a third which has yet to be fully imaged. The three galaxies (the first two of which are listed in Table 1) are NGC 1052 (an elliptical galaxy with a LINER nucleus), IRAS 22265, also known as TXFS 2226-184, originally classified as an elliptical or S0 but now definitely known to be a disk galaxy (Falcke et al. 2000a), and Mrk 348, classed as an S0. A fourth object, IRAS F01063-8034, which is definitely a disk galaxy, has a recently discovered maser (Greenhill et al. 2002) which also appears to be similar, and will be discussed briefly below.

These four objects stand out from the other megamasers on the basis of their line profiles. As noted in §1, the typical line profile for megamasers consists of a number of narrow components, with widths of a few km s⁻¹, spread over a much broader velocity range, $\Delta V \sim 10^2 - 10^3$ km s⁻¹. The four galaxies discussed in this section have completely different profiles, consisting of single, broad ($\Delta V \approx 90 - 130$ km s⁻¹, except for IRAS F01063, for which $\Delta V \approx 40 - 50$ km s⁻¹), more or less Gaussian lines. In the cases of NGC 1052 and Mrk 348, the maser emission is offset by approximately 150 km s⁻¹ with respect to the systemic velocity of the galaxy; no such offset has been reported for the IRAS 22265 emission and the IRAS F01063 emission is at the same velocity as the galaxy.

The spectral differences alone suggest that these masers differ in a fundamental way from the other megamaser sources. Imaging with VLBI appears to confirm this, at least for the first two mentioned. Claussen et al. (1998) presented VLBI observations of NGC 1052 in both 22 GHz continuum and the 6₁₆ - 5₂₃ water line. The continuum data show an elongated structure composed of at least seven components, with a gap near the center. The maser emission occurs in two moderately distinct groups, separated by about 0.02 pc, with a total extent of about 0.06 pc. Interestingly, the maser emission appears to lie along the axis of the “jet” seen in the continuum emission. There is also a clear velocity gradient in the maser emission, also in the direction parallel to the jet axis. The masers may be excited by shocks driven by the interaction of the jet with molecular clouds, as may be seen in the “jet masers” of NGC 1068 (Gallimore et al. 2001). Alternatively, given the superimposition of the masers on the continuum emission, the masers may arise in foreground molecular clouds that are amplifying the

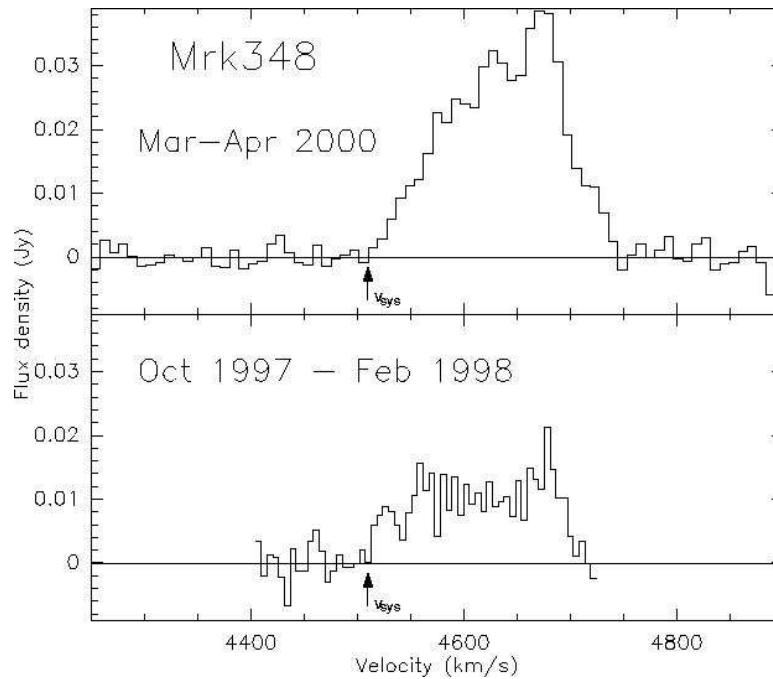


Figure 16: Spectrum of the maser emission from Mrk 348, at two different epochs. The maser clearly rose in intensity by a factor of three between late 1997 and early 2000. Also note the redshift of the emission with respect to the systemic velocity. From Falcke et al. (2000b).

continuum emission (although, given the very small angular and spatial scales involved, the absence of maser emission from the vicinity of the other continuum components is a little surprising in this interpretation). The latter scenario can be tested by searching for correlated variation of the continuum and maser emission (Claussen et al.), since for this model to work the maser emission must be unsaturated. The velocity centroid of the maser emission shifted by 45 km s^{-1} between two observations spaced five months apart (Braatz et al. 1996), which argues in favor of the jet-excited model.

IRAS 22265 has been imaged with VLBI but the results have not yet been published (Greenhill, Moran, & Henkel 2002, in preparation). In Moran et al. (1999), from which Table 1 has been adapted, the distribution of maser emission is described as “messy”, with a spatial extent of about 2.4 pc (note that their Table 3 contains a minor typographical error: the spatial extent of the emission in NGC 1052 is given as 0.6 pc rather than 0.06 pc). Greenhill et al. (2002) note that the emission from this source has been resolved into at least four components, spread over roughly a parsec, with individual line widths of tens of kilometers per second.

The third source with a single, broad maser line, Mrk 348, is a Seyfert 2 galaxy, with broad emission lines in polarized light. It is unusual among Seyfert galaxies in having a very bright and variable radio nucleus. Among the megamaser sources, in addition to its line profile, it is notable for having flared by about a factor of three in its 22 GHz emission (Falcke et al. 2000b), sometime between the end of 1997 and early

2000 (see Figure 16). It was observed but not detected in the Braatz et al. survey; analysis of archival observations by Falcke et al. show that it would have been seen only at the 3σ level at the time of the Braatz et al. observations. Furthermore, Falcke et al. present evidence that the radio continuum emission in Mrk 348 also rose between late 1997 and early 2000 by about the same factor as the maser emission. (Between early 1997 and late 1998, the flux density at 15 GHz was observed to increase by nearly a factor of 5 by Ulvestad et al. 1999.) If the variations of continuum and line are in fact correlated, this would indicate that the maser emission in Mrk 348 is unsaturated. The upper limit to the response time lag between the radio flare and the maser flare (about two years) sets an upper limit to the distance of the masers from the nucleus of about 0.6 pc. A recent VLBI observation with MERLIN (Xanthopoulos & Richards 2001) of the red half of the line observed by Falcke et al. confirms that maser emission arises within ~ 0.8 pc of one of the continuum peaks; the peak flux density is about three times higher than when observed by Falcke et al. (2000b), so that the maser flux density has increased by about an order of magnitude since late 1997.

The fourth source, IRAS F01063-8034, is a moderately distant (57 Mpc) southern edge-on disk galaxy, classified as Sa, which shows no real sign in the optical, infrared, or radio of possessing an active nucleus. Greenhill et al. (2002) discovered luminous ($L_{\text{H}_2\text{O}} \sim 450 L_\odot$) maser emission from this galaxy. The maser emission consists of a single Gaussian line, with a FWHM $\Delta V \approx 54 \text{ km s}^{-1}$. As in NGC 1052, the maser emission exhibited a shift in velocity, with the centroid jumping by 38 km s^{-1} within thirteen days. As with NGC 1052, such velocity shifts are difficult to understand except in the context of jet-excited models. In the case of IRAS F01063, this offers evidence for the presence of a previously unsuspected AGN in this galaxy.

The similarities among these four sources suggest that a common physical process is at work. The broad, smooth emission profiles may indicate that the maser action in all four of these galaxies is unsaturated, which would agree with the superimposition of the maser emission on the radio continuum source in NGC 1052, and with a correlated continuum/maser flare in Mrk 348. The spatial distribution of the emission, which is less cohesive than seen in most of the other megamasers imaged to date, may indicate a different origin than X-ray pumping, such as shocks, although this is not yet clear: both NGC 1052 and Mrk 348 are known to possess luminous ($L_x \sim 10^{42} - 10^{43} \text{ erg s}^{-1}$), heavily obscured ($N_H \sim 10^{23} \text{ cm}^{-2}$), nuclear hard X-ray sources (Weaver et al. 1999; Warwick et al. 1989). Certainly the velocity shifts seen in both NGC 1052 and IRAS F01063-8034 argue for a shock origin for the masers, perhaps due to jet/gas interactions.

6 The Future

Future, deeper surveys for H_2O megamasers can be expected to turn up many more sources in Seyfert 2 and LINER galaxies, given the known detection fractions (Braatz et al. 1996, 1997). Unfortunately, with existing instruments very few of these additional sources will be bright enough to image with VLBI; with the VLBA it is difficult (although not impossible, as discussed earlier) to observe sources that are fainter than about 0.5 Jy. The advent of the Atacama Large Millimeter Array (ALMA) will offer

a very large increase in sensitivity over the VLA. However, ALMA will not be able to observe the 22 GHz line, as the lower frequency limit will be 30 GHz, and, in any case, would not have the spatial resolution at this frequency (< 1 mas) required to image the nuclear maser emission in distant galaxies. The proposed Square Kilometer Array (SKA) will have a huge collecting area, and consequently enormous sensitivity at 22 GHz; hence SKA will be able to detect very faint, distant megamaser sources. However, it is not certain that SKA will be designed with the capability of performing high-resolution observations, in which case it will be superb for maser surveys but will not be able to do the follow-up imaging work. The Green Bank Telescope (GBT) will of course not have the necessary spatial resolution for imaging, but will be a superb instrument for monitoring studies.

However, imaging in the 22 GHz line is not the only method by which our understanding of H₂O megamasers can be improved. The only transition that has been observed so far from these sources is the $6_{16} - 5_{23}$ line at 22 GHz. However, a number of other water lines are predicted to maser, and several other masing transitions have been detected in Galactic sources: the $3_{13} - 2_{20}$ line at 183 GHz (Waters et al. 1980; Cernicharo et al. 1990); the $10_{29} - 9_{36}$ line at 321 GHz (Menten, Melnick, & Phillips 1990); and the $5_{15} - 4_{22}$ line at 325 GHz (Menten et al. 1990). In all of these sources the 22 GHz line is seen as well, and it is very likely that the maser radiation is arising in the same gas (e.g., the velocity range of emission is the same for all the transitions, except where detection is limited by low signal-to-noise; the line ratios seen in these sources, all of which are single-dish observations, are in reasonable agreement with model predictions; see Menten et al. 1990). All of these transitions are substantially weaker (both observationally and theoretically) than the 22 GHz line. However, the very large increase in sensitivity provided by ALMA will make it possible to observe the 321 and 325 GHz (and, under very favorable atmospheric conditions, the 183 GHz transition) from the ground. At 325 GHz, ALMA will have spatial resolution of 20 mas (assuming the planned 10 km baseline).

As discussed in Neufeld & Melnick (1991), observations of these transitions (and others that fall within the atmospheric windows) will make it possible to use masers not only as a probe of dynamics, but also of the physical conditions within the gas. Since these transitions arise at different energies above the ground and have different Einstein A values, the ratios of different masing transitions will depend on the density and temperature. Furthermore, by observing maser lines at different frequencies, it will be possible to determine whether free-free absorption is affecting the emission. For example, Herrnstein et al. (1996) proposed that the asymmetry between the redshifted and blueshifted high-velocity emission in NGC 4258 is not inherent, but is a consequence of the geometry (see Figure 6): on the redshifted side, it is the “underside” (from our perspective) of the disk that is irradiated, and so the warm, atomic zone lies behind the masing region, whereas on the blueshifted side they are reversed, and the maser emission is attenuated by free-free absorption within the weakly ionized atomic zone. This hypothesis can be tested by observing the disk at frequencies much higher than 22 GHz, where the optical depth to free-free emission becomes negligibly small. By observing density-sensitive line ratios, the actual densities in the masing zone can

be estimated, and compared with model predictions, such as the NM95 model. David Neufeld and I are currently at work on improved models of X-ray powered masers, to provide predictions of the line strengths and ratios for future observations.

Acknowledgments

My research on masers is supported by the National Science Foundation under grant AST 99-00871. This work was also supported by NASA through HST grant AR-08747.02-A. I wish to thank James Moran and a second, anonymous referee for their detailed and extremely helpful comments on a draft of this review, and Lincoln Greenhill and Jim Braatz for providing useful information. I am grateful to Brad Gibson and the ASA meeting organizers for the invitation to present the talk on which this article is based, and to Brad and Kristine and Joss and Sue for their hospitality in Melbourne and Sydney, respectively. Thanks to Joe for the company and all the driving in the 4WD monster and to Steve for just about everything else, especially the sushi and beer. Above all, I wish to thank Michelle Storey for her patience in dealing with this extremely late manuscript.

References

- Abramowicz, M.A., Chen, X., Kato, S., Lasota, J.-P., & Regev, O. 1995, *ApJ*, 438, L37
- Antonucci, R. 1993, *ARAA*, 31 473
- Baan, W.A., & Haschick, A.D. 1996, *ApJ*, 473, 269
- Balbus, S.A., & Hawley, J.F. 1991, *ApJ*, 376, 214
- Braatz, J.A., Wilson, A.S., & Henkel, C. 1997, *ApJS*, 110, 321
- Braatz, J.A., Wilson, A.S., & Henkel, C. 1996, *ApJS*, 106, 51
- Bragg, A.E., Greenhill, L.J., Moran, J.M., & Henkel, C. 2000, *ApJ*, 535, 73
- Brock, D., Joy, M., Lester, D.F., Harvey, P.M., & Ellis, H.B., Jr. 1988, *ApJ*, 329, 208
- Cecil, G., Bland-Hawthorn, J., Veilleux, S., & Filippenko, A.V. 2001, *ApJ*, 555, 338
- Cernicharo, J., Thum, C., Hein, H., John, D., Garcia, P., & Mattioco, F. 1990, *A&A*, 231, L15
- Cheung, A.C., Rank, D.M., Townes, C.H., Thornton, D.D., & Welch, W.J. 1969, *Nature*, 221, 626
- Churchwell, E., Witzel, A., Huchtmeier, W., Pauliny-Toth, I., Roland, J., & Suben, W. 1977, *A&A* 54, 969
- Claussen, M.J., & Lo, K.-Y. 1986, *ApJ*, 308, 592
- Claussen, M.J., Heiligman, G.M., & Lo, K.-Y. 1984, *Nature*, 310, 298
- Claussen, M.J., Diamond, P.J., Braatz, J.A., Wilson, A.S., & Henkel, C. 1998, *ApJ*, 500, L129
- Collison, A.J., & Watson, W.D. 1995, *ApJ* 452, L103
- Conway, J.E. 1999, in *Highly Redshifted Radio Lines*, Ed. C.L. Carilli, S.J.E. Radford, K.M. Menten, & G.I. Langston, (San Francisco: Astronomical Society of the Pacific),

- Curran, S.J., Johansson, L.E.B., Rydbeck, G., & Booth, R.S. 1998, *A&A*, 338, 863
- de Jong, T. 1973, *A&A*, 26, 297
- Desch, S.J., Wallin, B.K., & Watson, W.D. 1998, *ApJ*, 496, 775
- Done, C., Madejski, G.M., & Smith, D.A. 1996, *ApJ*, 463, L63
- dos Santos, P.M., & Lepine, J.R.D. 1979, *Nature*, 278, 34
- Duric, N., & Seaquist, E.R. 1988, *ApJ*, 326, 574
- Elitzur, M. 1992, *Astronomical Masers*, (Dordrecht: Kluwer), 262
- Elmouttie, M., Haynes, R.F., Jones, K.L., Sadler, E.M., & Ehle, M. 1998, *MNRAS*, 297, 1202
- Fairall, A.P. 1986, *MNRAS*, 218, 453
- Falcke, H., Wilson, A.S., Henkel, C., Brunthaler, A., & Braatz, J.A. 2000a, *ApJ*, 530, L13
- Falcke, H., Henkel, C., Peck, A.B., Hagiwara, Y., Almudena Prieto, M., & Gallimore, J.F. 2000b, *A&A*, 358, L17
- Fiore, F., Pellegrini, S., Matt, G., Antonelli, L.A., Comastri, A., della Ceca, R., Giallongo, E., Mathur, S., Molendi, S., Siemiginowska, A., Trinchieri, G., & Wilkes, B. 2001, *ApJ*, 556, 150
- Ford, H.C., Dahari, O., Jacoby, G.H., Crane, P.C., & Ciardullo, R. 1986, *ApJ*, 311, L7
- Frank, J., King, A., & Raine, D. 1992, *Accretion Power in Astrophysics* (2nd ed.) (Cambridge: Cambridge University Press)
- Gallimore, J.F., Baum, S.A., & O'Dea, C.P. 1997, *Nature*, 388, 852
- Gallimore, J.F., Baum, S.A., O'Dea, C.P., Brinks, E., & Pedlar, A. 1996, *ApJ*, 462, 740
- Gallimore, J.F., Henkel, C., Baum, S.A., Glass, I.S., Claussen, M.J., Prieto, M.A., & Von Kap-herr, A. 2001, 556, 694
- Gammie, C.F., Narayan, R., & Blandford, R. 1999, *ApJ*, 516, 177
- Gardner, F.F., & Whiteoak, J.B. 1982, *MNRAS*, 201, P13
- Genzel, R., & Downes, D. 1979, *A&A* 72, 234
- Greenhill, L.J. 2001a, in *Cosmic Masers*, ed. V. Migenes, (San Francisco: Astronomical Society of the Pacific), in press.
- Greenhill, L.J. 2001b, in *Proceedings of the 5th EVN Symposium*, ed. J. Conway, A. Polatidis, R. Booth, Onsala Space Observatory, Chalmers Technical University, Gothenburg, Sweden, in press.
- Greenhill, L.J., & Gwinn, C.R. 1997, *Ap&SS*, 248, 261
- Greenhill, L.J., Gwinn, C.R., Antonucci, R., & Barvainis, R. 1996, *ApJ*, 472, L21
- Greenhill, L.J., Moran, J.M., & Herrnstein, J.R. 1997a, *ApJ*, 481, L23
- Greenhill, L.J., Ellingsen, S.P., Norris, R.P., Gough, R.G., Sinclair, M.W., Moran, J.M., & Mushotzky, R. 1997b, *ApJ*, 474, L103
- Greenhill, L.J., Henkel, C., Becker, R., Wilson, T.L., & Wouterloot, J.G.A. 1995a, *A&A*, 304, 21
- Greenhill, L.J., Jiang, D.R., Moran, J.M., Reid, M.J., Lo, K.-Y., & Claussen, M.J. 1995b, *ApJ*, 440, 619
- Greenhill, L.J., Ellingsen, S.P., Norris, R.P., Gough, R.G., Sinclair, M.W., Moran,

- J.M., & Mushotzky, R. 1997, *ApJ*, 474, L103
- Greenhill, L.J., Moran, J.M., Booth, R.S., Ellingsen, S.P., McCulloch, P.M., Jauncey, D.L., Norris, R.P., Reynolds, J.P., Tzioumis, A.K., & Herrnstein, J.R. 2001, in *Galaxies and their Constituents at the Highest Angular Resolutions*, ed. R. Schilizzi, S. Vogel, F. Paresce, & M. Elvis (San Francisco: Astronomical Society of the Pacific), in press.
- Greenhill, L.J., Moran, J.M., & Henkel, C. 2002, in preparation.
- Hagiwara, Y., Diamond, P.J., & Miyoshi, M. 2002, *A&A*, 383, 65
- Hagiwara, Y., Kohno, K., Kawabe, R., & Nakai, N. 1997, *PASJ*, 49, 171
- Haschick, A.D., & Baan, W.A. 1985, *Nature*, 314, 144
- Haschick, A.D., Baan, W.A., & Peng, E.W. 1994, *ApJ*, 437, L35
- Heckman, T.M. 1980, *A&A*, 87, 152
- Henkel, C., Güsten, R., Thum, C., & Downes, D. 1984a, *IAU Circ.* 3983
- Henkel, C., Güsten, R., Wilson, T.L., Biermann, P., Downes, D., & Thum, C., 1984b, *A&A*, 141, L1
- Herrnstein, J.R. 1997, Ph.D. Thesis, Harvard University
- Herrnstein, J.R., Greenhill, L.J., & Moran, J.M. 1996, *ApJ*, 468, L17
- Herrnstein, J.R., Moran, J.M., Greenhill, L.J., Blackman, E.G., & Diamond, P.J. 1998, *ApJ*, 508, 243
- Herrnstein, J.R., Greenhill, L.J., Moran, J.M., Diamond, P.J., Inoue, M., Nakai, N., & Miyoshi, M. 1998, *ApJ*, 497, L69
- Herrnstein, J.R., Moran, J.M., Greenhill, L.J., Diamond, P.J., Miyoshi, M., Nakai, N., & Inoue, M. 1997, *ApJ*, 475, L17
- Herrnstein, J.R., Moran, J.M., Greenhill, L.J., Diamond, P.J., Inoue, M., Nakai, N., Miyoshi, M., Henkel, C., & Riess, A. 1999, *Nature*, 400, 539
- Ichimaru, S. 1977, *ApJ*, 214, 840
- Ishihara, Y., Nakai, N., Iyomoto, N., Makishima, K., Diamond, P., & Hall, P. 2001, *PASJ*, 53, 215
- Iyomoto, N., Fukazawa, Y., Nakai, N., & Ishihara, Y. 2001, *ApJ*, 561, L69
- Iwasawa, K., Koyama, K., Awaki, H., Kunieda, H., Makishima, K., Tsuru, T., Ohashi, T., & Nakai, N. 1993, *ApJ*, 409, 155
- Kartje, J.F., Königl, A., & Elitzur, M. 1999, *ApJ*, 513, 180
- Koekemoer, A.M., Henkel, C., Greenhill, L.J., Dey, A., van Breugel, W., Codella, C., & Antonucci, R. 1995, *Nature*, 378, 697
- Lasota, J.-P., Abramowicz, M.A., Chen, X., Krolik, J., Narayan, R., & Yi, I. 1996, *ApJ*, 462, 142
- Madejski, G.M., Życki, P., Done, C., Valinia, A., Blanco, P., Rothschild, R., & Turek, B. 2000, *ApJ*, 535, L87
- Makishima, K., Fujimoto, R., Ishisaki, Y., Kii, T., Loewenstein, M., Mushotzky, R., Serlemitsos, P., Sonobe, T., Tashiro, M., & Yaqoob, T. 1994, *PASJ*, 46, L77
- Maloney, P.R., Begelman, M.C., & Pringle, J.E. 1996, *ApJ*, 472, 582
- Maloney, P.R., Hollenbach, D.J., & Tielens, A.G.G.M. 1996, *ApJ* 466, 561
- Maoz, E. 1995, *ApJ*, 447, L91
- Maoz, E., & McKee, C. F. 1998, *ApJ*, 494, 218

- Marconi, A., Moorwood, A.F.M., Origlia, L., & Oliva, E. 1994, *Messenger*, 78, 20
- Matt, G., Fiore, F., Perola, G.C., Piro, L., Fink, H.H., Grandi, P., Matsuoka, M., Oliva, E., & Salvati, M. 1996, *MNRAS*, 281, L69
- Menten, K.M., Melnick, G.J., & Phillips, T.G. 1990, *ApJ*, 350, L41
- Menten, K.M., Melnick, G.J., Phillips, T.G., & Neufeld, D.A. 1990, *ApJ*, 363, L27
- Miyoshi, M., Moran, J., Herrnstein, J., Greenhill, L., Nakai, N., Diamond, P., & Inoue, M. 1995, *Nature*, 373, 127
- Moran, J.M., Greenhill, L.J., & Herrnstein, J.R. 1999, *J. Astrophys. Astron.*, 20, 165
- Moran, J., Greenhill, L., Herrnstein, J., Diamond, P., Miyoshi, M., Nakai, N., & Inoue, M. 1995, in *Quasars and AGN: High Resolution Imaging*, *Proc. Nat. Acad. Sci.*, 92, 11427
- Nakai, N., Inoue, M., & Miyoshi, M. 1993, *Nature*, 361, 45
- Nakai, N., Inoue, M., Miyazawa, K., & Hall, P. 1995, *PASJ* 47, 771
- Nakai, N., Sato, N., & Yamauchi, A. 2002, *PASJ*, 54, in press.
- Narayan, R., & Yi, I. 1994, *ApJ*, 428, L13
- Neufeld, D.A. 2000, *ApJ*, 542, L99
- Neufeld, D.A., & Maloney, P.R. 1995, *ApJ*, 447, L19
- Neufeld, D.A., Maloney, P.R., & Conger, S. 1994, *ApJ*, 436, L127
- Neufeld, D.A., & Melnick, G.J. 1991, *ApJ*, 368, 215
- Newman, J.A., Ferrarese, L., Stetson, P.B., Maoz, E., Zepf, S.E., Davis, M., Freedman, W.L., & Madore, B.F. 2001, *ApJ*, 553, 562
- Phinney, E.S. 1983, Ph.D. Thesis, University of Cambridge
- Pringle, J.E. 1996, *MNRAS*, 281, 357
- Rees, M.J., Begelman, M.C., Blandford, R.D., & Phinney, E.S. 1982, *Nature*, 295, 17
- Reynolds, C.S., Nowak, M.A., & Maloney, P.R. 2000, *ApJ*, 540, 143
- Sawada-Satoh, S., Inoue, M., Shibata, K.M., Kamenno, S., Migenes, V., Nakai, N., & Diamond, P.J. 2000, *PASJ*, 52, 421
- Shakura, N.I., & Sunyaev, R.A. 1973 *A&A* 24, 337
- Stone, J.M., Hawley, J.F., Gammie, C.F., & Balbus, S.A. 1996, *ApJ*, 463, 656
- Svensson, R. 1999, in *Theory of Black Hole Accretion Discs*, ed. M.A. Abramowicz, G. Bjornsson, and J.E. Pringle, (Cambridge: Cambridge University Press), 289
- Tielens, A.G.G.M., & Hollenbach, D.J. 1985, *ApJ*, 291, 722
- Trotter, A.S., Greenhill, L.J., Moran, J.M., Reid, M.J., Irwin, J.A., & Lo, K.-Y. 1998, *ApJ*, 495, 470
- Ulvestad J.S., Wrobel J.M., Roy A.L., Wilson, A.S., Falcke, H., & Krichbaum, T.P. 1999, *ApJ*, 517, L81
- Veilleux, S., & Bland-Hawthorn, J., 1997 *ApJ*, 479, L105
- Warwick, R.S., Koyama, K., Inoue, H., Takano, S., Awaki, H., & Hoshi, R. 1989, *PASJ*, 41, 709
- Waters, J.W., Kakar, R.K., Kuiper, T.B.H., Roscoe, H.K., Swanson, P.N., Rodriguez Kuiper, E.N., Kerr, A.R., Thaddeus, P., & Gustincic, J.J. 1980, *ApJ*, 235, 57
- Weaver, K.A., Wilson, A.S., Henkel, C., & Braatz, J.A. 1999, *ApJ*, 520, 130
- Whiteoak, J.B. & Gardner, F.F., 1986, *MNRAS*, 222, 513
- Xanthopoulos, E., & Richards, A.M.S. 2001, *MNRAS*, 326, L37

TABLE 1^a
WATER MEGAMASERS OBSERVED WITH VLBI

Masers With Disk Structure							
Galaxy	D Mpc	v_ϕ km/s	R_i/R_o pc	M $10^6 M_\odot$	ρ $10^7 M_\odot/\text{pc}^3$	L_x 10^{42} erg/s	Reference
NGC 4258	7	1100	0.13/0.26	39	400	0.04	M95
NGC 1068	15	330	0.6/1.2	17	3	40	GG97
Circinus	4	230	0.08/0.8	1	40	40	G01
NGC 4945	4	150	0.2/0.4	1	2	6	G97
NGC 1386	12	100	–/0.7	2	4	0.02	B99
NGC 3079	16	150	–/1.0	1	0.2	1–10	T98, S00
IC 2560 ^b	26	420	0.07/0.26	3	210	0.1	I01

Masers Without Obvious Disk Structure						
Galaxy	D Mpc	v_0 km/s	Δv km/s	ΔR pc	Comment	Reference
IRAS 22265 (S0)	100	7570	150	2.4	messy	G02
NGC 1052 (E4)	20	1490	100	0.06	“jet”	C98

^aAdapted and updated from Moran, Greenhill, & Herrnstein (1999)

D = distance, v_0 = systemic velocity, Δv = velocity range, ΔR = linear extent, v_ϕ = rotational velocity, R_i/R_o = inner/outer radius of disk, M = central mass, ρ = central mass density, L_x = X-ray luminosity.

^bOnly the systemic velocity emission in IC 2560 has been imaged; it is included here because of kinematic evidence for a rotating disk (Ishihara et al. 2001). See discussion in text.

References: G02 = Greenhill et al. 2002, C98 = Claussen et al. 1998, I01 = Ishihara et al. 2001, M95 = Miyoshi et al. 1995, GG97 = Greenhill & Gwinn 1997, G01 = Greenhill et al. 2001, G97 = Greenhill et al. 1997, B99 = Braatz et al. 1999, T98 = Trotter et al. 1998, S00 = Sawada-Satoh et al. 2000